

Review

Ruthenium Complexes as Sensitizers in Dye-Sensitized Solar Cells

Sadig Aghazada  and Mohammad Khaja Nazeeruddin *

Group for Molecular Engineering of Functional Materials, École Polytechnique Fédérale de Lausanne, Valais Wallis, CH-1951 Sion, Switzerland; sadig.aghazada@epfl.ch

* Correspondence: mdkhaja.nazeeruddin@epfl.ch; Tel.: +41-(0)21-695-8251

Received: 27 April 2018; Accepted: 17 May 2018; Published: 21 May 2018



Abstract: In this review, we discuss the main directions in which ruthenium complexes for dye-sensitized solar cells (DSCs) were developed. We critically discuss the implemented design principles. This review might be helpful at this moment when a breakthrough is needed for DSC technology to prove its market value.

Keywords: ruthenium complexes; dye-sensitized solar cells; solar energy; cyclometalated complexes

1. Introduction

The annual global temperature keeps rising in parallel with the increasing concentration of carbon dioxide in the atmosphere (Figure 1). Both of these processes are consequences of extensive use of fossil fuels to meet humanity's energy demand. To prevent further disturbances of the atmosphere, the move toward carbon-dioxide-free sources of energy is required [1,2]. Use of solar panels together with fuel cells or batteries should help in this transition. Many types of solar cells have been developed in research laboratories and some are on the market. Among these technologies are dye-sensitized solar cells (DSCs), which were under intense scrutiny for three decades [3,4]. DSC uses a wide band-gap semiconductor material, which is sensitized to visible light by a dye molecule on its surface. Various complexes of ruthenium were extensively used as a dye in both small area devices and big area panels. In this critical review article, we will discuss ruthenium complexes that were utilized to improve the performance of solar cells. We will go through the design principles that researchers implemented to obtain a well-performing sensitizer and to discuss which of these principles are valid after three decades. However, this paper will first describe the working concept of a DSC.

In their most conventional architecture, a small-area DSC is made of a photoanode with a cathode sandwiching liquid electrolyte in between. The photoanode is made of a glass covered with a film of transparent conductive oxide. This glass is covered with the blocking and mesoporous layers of semiconductor, most frequently titania, and the semiconductor is then covered with a monolayer of dye molecules. The cathode is usually made of the same conductive glass as in the photoanode with deposited on top it particles of a solid catalyst [5]. The liquid electrolyte is made of a solution of redox mediator in an organic solvent and contains various additives. In an ideal case, the dye molecule (S) absorbs the incident photon of high enough energy, and ends up in the electronically excited state (S^*). Excited dye molecules inject their electrons into the conduction band of semiconductor filling up the present trap states, and remain in the oxidized state (S^+). The reduced components of a redox mediator in the electrolyte (I^- , Co^{2+} , Cu^{1+} , etc.) reduce the oxidized dye molecule (S^+), and a hole (h as I_3^- , Co^{3+} , Cu^{2+} , etc.) in the electrolyte diffuses to the counter electrode. At the same time, electrons in the titania are collected and path through an external circuit and reach the counter electrode. The recombination of electrons and holes at the counter electrode closes the circuit. In reality, additional destructive processes are taking place. Among them, related to the photoanode-electrolyte

interface are: (i) electronic relaxation of an excited sensitizer to its ground state; (ii) electron-oxidized sensitizer recombination; and (iii) electron-electrolyte recombination. One can design sensitizers to hamper these destructive pathways.

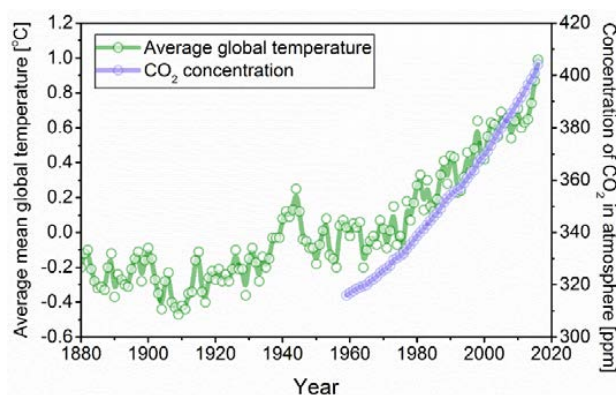


Figure 1. The rise in average global temperatures and CO₂ concentrations in the atmosphere. The graph was built based on data from NASA's Goddard Institute for Space Studies (NASA/GISS) and from Dr. Pieter Tans, National Oceanic and Atmospheric Administration at Earth System Research Laboratory (NOAA/ESRL) (www.esrl.noaa.gov/gmd/ccgg/trends/) and Dr. Ralph Keeling, Scripps Institution of Oceanography (scrippsco2.ucsd.edu/).

2. Sensitizers

It worth noting that the oxidation potentials mentioned below are implied versus the normal hydrogen electrode (NHE) potential unless otherwise noted.

For an efficient DSC, a sensitizer should meet the following requirements:

1. The sensitizer should possess an anchoring group, which should enable efficient chemisorption of sensitizer onto the mesoporous oxide. Most of the developed sensitizers possess carboxylic and phosphonic acid anchors; however, impressive results were recently presented with silyl-anchors [6].

2. For an efficient dye-regeneration, the oxidation potential of the sensitizer should be higher than the oxidation potential of a redox couple that immediately regenerates it. The efficient regeneration implies two orders of magnitude faster regeneration than charge recombination with a photooxidized sensitizer. For a DSC with an electrolyte based on an outer-sphere one-electron redox mediator like [Co(bpy)₃]^{3+/2+} and [Cu(bpy)₂]^{2+/1+}, the regeneration kinetics are well described by Marcus' electron transfer theory, where the two main factors that determine the rate of electron transfer are the driving force $\Delta G = -nF\Delta E$, and the reorganization energy $\Lambda = \lambda_{\text{inner}} + \lambda_{\text{out}}$ [7–9]. Thus, depending on the nature of the redox mediator, the necessary driving force for the efficient regeneration may vary depending on the reorganization energy. On the other hand, the exact couple that participates in direct regeneration in the iodine-based electrolyte is not yet established and may vary depending on the sensitizer.

3. The sensitizer's excited state oxidation potential should be more cathodic than the conduction band edge of titania. As Gerischer developed, the rate of electron injection from a sensitizer into the electrode is described as $k \propto \int \kappa_{\text{don}}(E)D(E)W_{\text{don}}(E)dE$, where $\kappa_{\text{don}}(E)$ is a transfer frequency as a function of E , $D(E)$ is a density of empty electron states (DOS) within a semiconductor, and $W_{\text{don}}(E)$ is a density of electron donor states referred to sensitizers [10–12]. Thus, for the fast charge injection, the density of donor states, $W_{\text{don}}(E)$, which, in our case, is the population density of the vibrational states for the excited sensitizer S^* , and DOS should overlap in energy. As illustrated in Figure 2, W_{don} reaches its maxima at potentials below the sensitizers excited state potential by λ/e , which implies that for a fast charge injection the excited state potential should be at least few hundreds of mV more cathodic than the conduction band edge of mesoporous oxide.

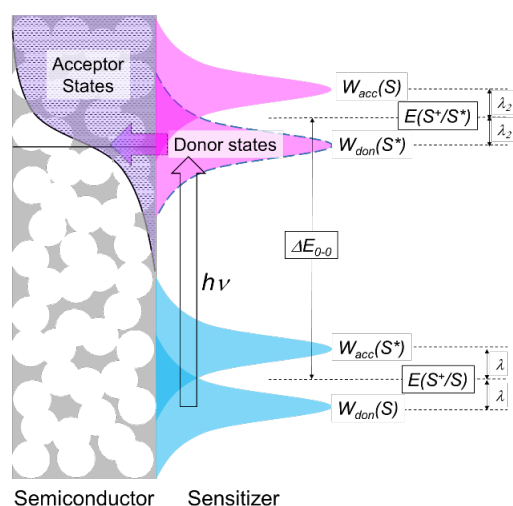


Figure 2. A Gerischer diagram illustrating electron injection from the photo-excited sensitizer into the acceptor states within titania [10–12].

4. The absorption spectrum for a sensitizer should be intense to absorb most of the light on a thin layer of sensitized mesoporous titania film. Roughly, extinction coefficients above $10^4 \text{ M}^{-1} \cdot \text{cm}^{-1}$ are desired. However, sensitizers with lower extinction coefficients still work well when a thick film of mesoporous layer is used.

5. For a record efficient DSC, a sensitizer should absorb all the photons up to 940 nm [13], which implies very high Highest Occupied Molecular Orbital (HOMO) and very low Lowest Unoccupied Molecular Orbital (LUMO) energies. Thus, for this sensitizer, the overpotentials required for efficient regeneration and charge injection should be exceptionally small.

6. For the efficient sensitizer, the HOMO and LUMO should be spatially separated, with the LUMO close to the part of molecule with the anchoring group and the HOMO on the part further away from the oxide surface. The closeness of the LUMO to the oxide surface is advantageous for efficient charge injection, while a HOMO far away from the semiconductor surface is useful for two reasons. First, it is necessary to hamper the rate of malignant charge recombination with the photooxidized sensitizer, and second, it increases the visibility of a hole for the electron donors in the electrolyte.

7. The sensitizer should be photochemically and electrochemically stable. For the DSC to be stable for 20 years, the oxidation–back-reduction turnover number for the sensitizer should be above 10^6 .

From the early ages of DSCs, derivatives of ruthenium(II) bipyridine complexes were extensively employed showing good performances. However, their popularity in the DSC field might be just a result of the fact that they had been already at forefront of attention due to their interesting photophysical and electrochemical characteristics. As a result, most of the theoretical bases for DSCs were built studying devices with ruthenium sensitizers and very little attention was given to other possibilities, except much later, to organic sensitizers. Below, we will start discussing the main feature of ruthenium complexes that made them to stand out, which is their characteristic metal-to-ligand charge transfer. Afterwards, we will describe some of the ruthenium sensitizers that played important roles in development of DSCs. In contrast to some present reviews, we will also add some of our thoughts into the discussion [14,15].

3. Ruthenium Complexes

To understand the possible ways of controlling the Metal-to-Ligand Charge Transfer (MLCT) band of ruthenium bipyridine complexes, we would like to revise its origin. For that, we need to bring the molecular orbital diagram for simplest ruthenium(II) *tris*-bipyridine complex $\text{Ru}(\text{bpy})_3^{2+}$ to show how the central atom's *s*, *p*, and *d* orbitals σ - and π -interact with ligands' group orbitals.

Although $\text{Ru}(\text{bpy})_3^{2+}$ has a D_3 symmetry, we may assume that σ -donating ligand orbitals, simply the lone electron pairs on nitrogens, create an octahedral environment around the central atom. This is almost true except that in $\text{Ru}(\text{bpy})_3^{2+}$ the $\angle\text{NRuN}$ angles for *cis*-nitrogens are not equal to 90° . Thus, in the octahedral environment, ruthenium's one *s* and three *p* atomic orbitals will gain A_{1g} and T_{1u} representations respectively, while five *d* atomic orbitals will split into set of two groups of T_{2g} and E_g representation. Analogously, six σ -donating ligand orbitals in the O_h environment will split into three set of group orbitals with A_{1g} , T_{1u} , and E_g representations. As shown in Figure 3, all the ruthenium orbitals, except those with T_{2g} representation, have matching ligand counterparts to interact with, resulting in bonding and antibonding molecular orbitals. However, the t_{2g} orbitals remain nonbonding. Six Ru(II) *d* electrons together with 12 electrons from the 6 σ -ligands will fill all six bonding orbitals and three t_{2g} nonbonding orbitals. Considering that the bonding orbitals are too deep in energy, they do not play any crucial role in the photophysical and electrochemical properties of the complex. However, the positions of non-bonding t_{2g} and antibonding e_g^* orbitals are one of the most important factors for the complex. Thus, this diagram implies that the donating nature of σ -ligand orbitals affects only the e_g^* orbital and that by varying the basicity of ligand orbitals and their overlap with the central atom orbitals, only the e_g^* orbital energy can be controlled.

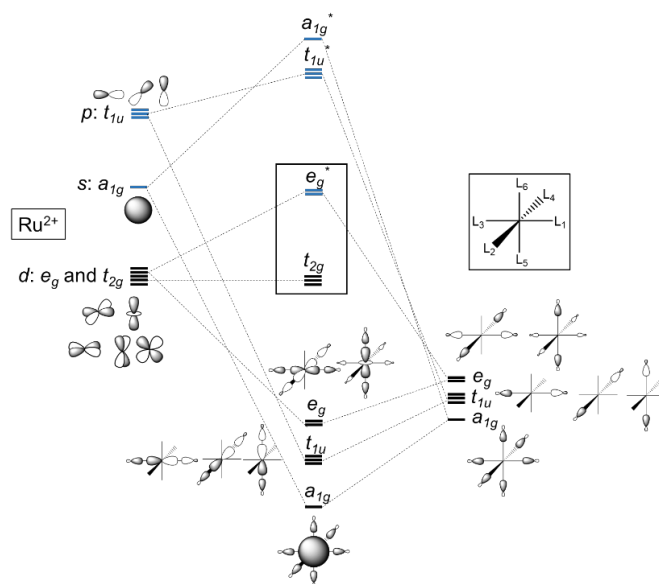


Figure 3. The interaction diagram of Ru^{2+} ions with six identical σ -ligands in an O_h symmetry point group. Bonding interactions of symmetry-adapted linear combination of ligand donor orbitals with metal orbitals are presented. Black and blue bars represent doubly filled and empty orbitals, respectively.

In addition to the σ -donation from six nitrogens, $[\text{Ru}(\text{bpy})_3]^{2+}$ has an aromatic orbitals on each pyridine ring, which may interact with the central atom. Instead of building a D_3 symmetry-adapted linear combination of ligand π -orbitals and constructing their interaction with a central atom, we could just qualitatively check how ligand π -orbitals are interacting with the central atom orbitals. Among the t_{2g} and e_g^* orbitals that are already formed as a result of interactions with the σ -ligands, only t_{2g} orbitals may π -interact with the ligand orbitals. In Figure 4, a perturbation of t_{2g} orbitals as a result of the interaction with the π -acidic and π -basic ligands is presented. Both types of ligands could be present in sensitizers, with pyridine, NCS, and cyclometalated ligands as π -basic, and *N*-heterocyclic-carbenes as π -acidic ligands. In the case of pyridine-type ligands, the bonding t_{2g} orbitals will be filled with the ligand orbitals and the antibonding t_{2g}^* orbitals will be filled with six electrons from the Ru(II). Since the energy difference between the metal t_{2g} and ligand t_{2g} group orbitals is usually high, the π -bonding

is usually weak, resulting in the bonding and antibonding t_{2g} orbitals having primarily ligand and metal orbital nature, respectively. Consequently, the metal-to-ligand charge transfer occurs from the generally metal-based t_{2g}^* orbitals to the ligand-based π^* orbitals.

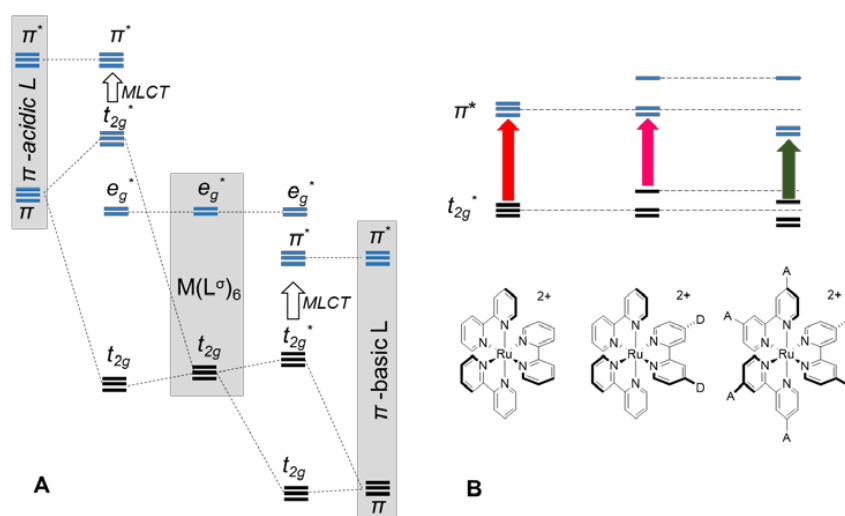


Figure 4. (A) An interaction of π -acidic and π -basic ligand orbitals with metal-based orbitals formed as a result of the interaction with six σ -ligands (vide supra Figure 3). (B) The effect of π -donor and π -acceptor substituents on the molecular orbital energies in heteroleptic ruthenium(II) complexes. D and A stand for π -donating and accepting substituents. The black and blue bars represent doubly filled and empty orbitals, respectively.

As follows from the interaction diagram in Figure 4, by tuning the π -basicity of the ligand orbitals, one may control the t_{2g}^* orbital energy and thus control the MLCT band energy. However, complete control over MLCT band position is not possible, since ligand's π^* -orbital energy changes in accord with its π -basicity. In heteroleptic complexes, various ligands with different π -basicity can be used to bypass this problem, as illustrated in Figure 4B with derivatives of $[\text{Ru}(\text{bpy})_3]^{2+}$. When the π -basicity values of various ligands are differentiated, the highest energy t_{2g}^* and the lowest energy π^* orbitals originate from the ligands of the highest and lowest π -basicity values, respectively. Thus, primarily the strongly π -donating ligands control the position of the t_{2g}^* orbital, while weaker π -donating ligands are responsible for the π^* -orbitals that participate in the lowest-energy MLCT band. In addition to controlling the energy of the MLCT band, differentiation of ligands also attribute directionality to the MLCT band. This directionality of the MLCT bands in heteroleptic ruthenium complexes is one of the factors that determines their success in DSCs (vide supra: requirements for sensitizers: point 6).

The absorption spectrum of $[\text{Ru}(\text{bpy})_3]^{2+}$ exhibits a set of MLCT $\pi_M-\pi_L^*$ (MLCT) bands in the visible region of solar spectrum and a set of ligand centered (LC) $\pi_L-\pi_L^*$ bands in the UV part. Above we have discussed the interaction of ruthenium t_{2g} orbitals with ligand π^* -orbitals in the octahedral microsymmetry of D_3 . However, as Orgel noted, in a D_3 point group, the originally t_2 orbitals split into two: degenerate e and not-degenerate a_1 [16]. Reduction of symmetry results in additional MLCT transitions.

As was stated above, for the efficient chemisorption, a sensitizer should possess anchoring groups. In 1985 Desilvestro et al. used *tris*-(4,4'-dicarboxy-2,2'-bipyridine) ruthenium(II) dichloride $[\text{Ru}(\text{dc-bpy})_3]\text{Cl}_2$ to sensitize titania of fractal morphology. For comparison, authors also sensitized films with $[\text{Ru}(\text{bpy})_3]^{2+}$. The former provided then exceptionally high photon-to-current conversion efficiency reaching 44%, while the latter provided only 2.7% [17]. Later, with $[\text{Ru}(\text{dc-bpy})_3]^{2+}$ sensitized fractal titania, Vlachopolous et al. reported IPCE values reaching 73% and PCE of 12% with incident light power of only 0.632 mW. As we mentioned above, for an efficient sensitizer, directionality for

charge transfer is desired. This is not the case for the homoleptic ruthenium complexes, and yet $[\text{Ru}(\text{dc-bpy})_3]^{2+}$ provided surprisingly 94% efficient charge injection [18]. This highly efficient injection may indicate on two pathways: (a) first, photoexcited sensitizer may efficiently inject its electron into the conduction band of titania while still in vibrationally hot states; and/or (b) relaxed to the MLCT state molecule has the excited electron on the bpy ligand directly attached to titania surface. Later, with *bis*-heteroleptic ruthenium complex $[\text{Ru}(\text{dcbpy})_2(\text{H}_2\text{O})_2]^{2+}$ (precipitated at its isoelectric point) on a fractal titania, promising results were obtained as well, with Incident Photon-to-current Conversion Efficiency IPCE and injection efficiency reaching 60% and 62% respectively [19]. However, the comparison of sensitizers' performances obtained with fractal titania and not-optimized electrolytes is counterproductive.

In their seminal paper in 1991 [3], Brian O'Regan and Michael Grätzel introduced new mesoporous titania with roughness factor ca. 1000. In this work, cyano-bridged trinuclear ruthenium complex developed before by Amadelli et al. [20], on the mesoporous titania provided PCE over 7% (Figure 5). In this complex, two "antenna" ruthenium complexes $\text{Ru}(\text{bpy})_2(\text{CN})_2$ are attached to the anchoring $\text{Ru}(\text{dc-bpy})_2$ moiety via cyano-groups, and the former may efficiently transfer their absorbed energy to the latter. This complex possesses two apparent broad absorption bands in the visible region of solar spectrum, the high energy one was related to the MLCT in the peripheral "antennas", and the low-energy band was related to the MLCT in the central moiety. With this complex, only one emission band related to the central moiety was observed, and in the time-correlated single photon counting measurement no rise-time was observed, indicating that efficient energy transfer from the peripheral moieties to the central anchoring moiety is taking place within 10^{-9} s as defined by instrument [20]. However, multinuclear complexes bridged with monodentate ligand usually tend to dissociate rendering them unpromising for long-term application in DSCs.

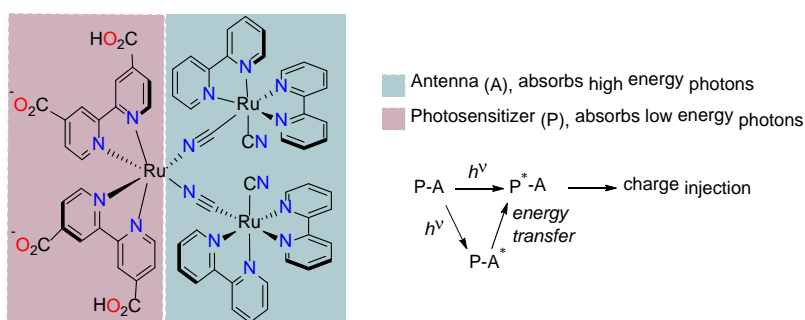


Figure 5. Trinuclear ruthenium complex. Antenna moieties improve light absorption in high energies.

3.1. Ruthenium Complexes with Isothiocyanate Ligands

In 1993, Nazeeruddin et al. introduced a series of *bis*-heteroleptic ruthenium complexes $\text{cis-Ru}(\text{dc-bpy})_2\text{X}_2$, where $\text{X} = \text{Cl}^-$, Br^- , I^- , CN^- , and SCN^- [21]. Among these complexes, the isothiocyanate-substituted one, named N3 sensitizer, exhibited the most promising characteristics: (i) broad absorption spectrum with high extinction coefficient; (ii) relatively long excited state lifetime to ensure efficient charge injection into the conduction band of titania; and suitable oxidation potential for efficient sensitizer regeneration when an electrolyte based on I_3^-/I^- redox is employed. In this work, PCE of 10% was achieved. Moreover, authors showed that dipping electrodes into 4-*t*-butyl-pyridine increases the V_{OC} from 380 to 660 mV, which was related to the passivation of surface Ti(IV) states, leading to reduced charge recombination.

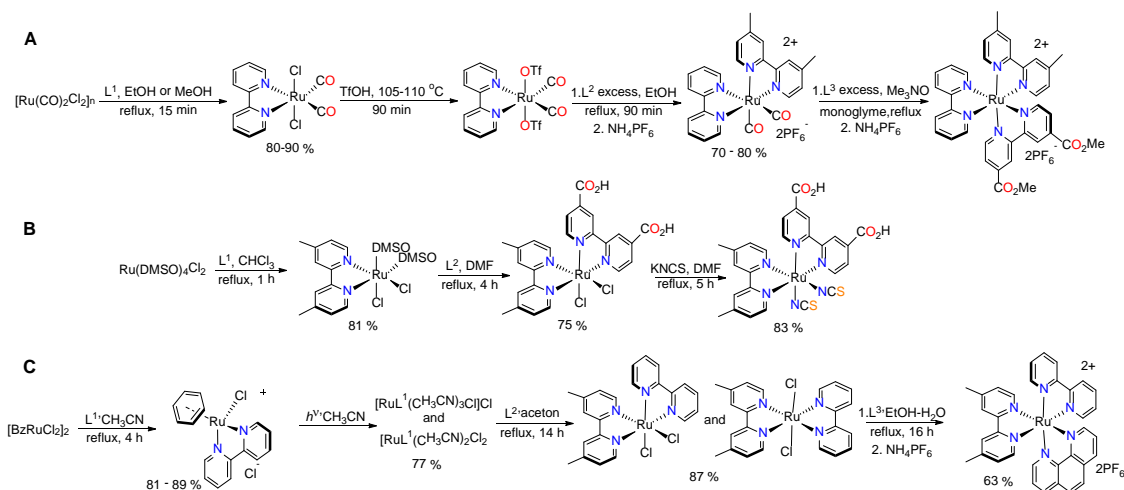
Another advantageous feature of N3 sensitizer is that its frontier-occupied orbitals are composed of antibonding interaction between the Ru t_2 and isothiocyanate π^* orbitals. The unoccupied frontier orbitals generally consist of 4,4'-dicarboxy-2,2'-bipyridine π^* orbitals. Such a spatial separation of occupied and empty frontier orbitals does not only facilitate efficient charge injection and

dye-regeneration as was mentioned above, but also enables control over the absorption spectra and electrochemical parameters of the complex. For example, deprotonation of acid groups in N3 sensitizer drastically influences both the absorption spectra and the oxidation potential in two ways: (a) deprotonation results in increased energy of π^* orbitals; and (b) deprotonation increases the π -basicity of bipyridine ligands. According to the cyclic voltammetry measurements, both the oxidation and reduction potentials, which are qualitatively related to the HOMO and LUMO energies, shift cathodically with deprotonation [22]. Apart from the effects on the intrinsic characteristics of a sensitizer, its protonation degree also impacts the electronic properties of mesoporous semiconductor. As the conduction band edge of mesoporous oxide shifts anodically with reduction of pH, the fully protonated N3 sensitizer and fully deprotonated N3 sensitizer provide different performances [23–26]. Protonated N3 sensitizer causes downward shift of the conduction band edge and thus provides lower V_{OC} and higher J_{SC} than the fully deprotonated N3 sensitizer. The compromise between V_{OC} and J_{SC} can be achieved with partially deprotonated N3 sensitizer. The double deprotonated version of N3 sensitizer, was presented later and named as N719 [27]. Solar cells with this sensitizer provided PCE of 11.18%. In the same work, with the help of Density-Functional Theory (DFT) and Time Dependents-DFT (TD-DFT) calculations, authors calculated the electronic energy levels for the N3 sensitizer and for its partially and fully deprotonated analogues, among which is N719. Authors claim that double- and single-protonated complexes provide optimal compromise between the molecule optical band gap and LUMO energy, and that in N3 sensitizer the LUMO is too low to enable efficient charge injection. The PCE of 11.18% was achieved with monoprotonated sensitizer obtained by adding one equivalent of chenodeoxycholic acid salt to the electrolyte sensitized with N719. This claim asks for further questions: (i) although chenodeoxycholic acid is basic enough to deprotonate the N719, one would expect protons to attach onto the titania; and (ii) chenodeoxycholic acid may simply passivate free active sites on titania surface, reducing charge recombination. The latter is likely responsible for efficiency improvement, since it was achieved mostly due to the improvement in V_{OC} with insignificant changes in J_{SC} .

According to the Shockley-Queisser analysis, ideally, a single-junction solar cell should provide a power conversion efficiency little over 30% [13]. For this high efficiency, the solar cell should absorb all the incident photons with energy higher than 1.1 eV. For the N719 sensitizer with the absorption onset of 780 nm (1.59 eV) the voltage of 846 mV was obtained, indicating that loss-in-potential is 0.744 eV. To improve the efficiency of DSC both the optical bandgap and loss-in-potential should be reduced. Most of loss-in-potential come from the two processes: (a) high regeneration overpotential with I_3^-/I^- -based electrolyte; and (b) necessary driving force for charge injection into titania. Shrinking the optical bandgap of sensitizer implies reduction of both overpotentials required for regeneration and charge injection. As Snaith underlined, one of the reasons for high driving force necessary for efficient charge injection is the heterogeneity in injection rates [28]. Many studies support that for N719 few charge injection pathways in fs and ps timescale take place, among which are injection from: vibrationally hot states, 1MLCT , and 3MLCT states [12,29–31]. Thus, the conduction band edge should be deep enough to ensure that the slowest injection is also complete. However, as Nazeeruddin et al. showed, a new N749 sensitizer, which is due to its appearance in solid state is also known as “black dye”, has an optical bandgap of 1.38 eV (900 nm) and suffers from lower loss-in-potential of 0.66 eV than N719 [32]. In black dye, ruthenium is coordinated with three donating isothiocyanate ligands and anchoring tridentate 2,2':6',2''-terpyridine functionalized with three carboxy-groups at 4, 4', and 4'' positions. This new complex was synthesized in two step procedures from a ruthenium trichloride hydride and 4,4',4''-tricarboxy-2,2':6',2''-terpyridine and two of the carboxylic acid groups were then deprotonated. For comparison, analogues with either all protonated or all deprotonated carboxylic groups were also prepared. Among these three sensitizers, N749 with two deprotonated carboxylic groups provided the highest PCE of 10.4%, mostly due to high J_{SC} reaching $20.5 \text{ mA}\cdot\text{cm}^{-2}$ [32].

Apart from the *bis*-heteroleptic ruthenium complexes like N3, N719, and black dye, their *tris*-heteroleptic complexes were also developed. Synthesis of *tris*-heteroleptic ruthenium

complexes with 2,2'-bipyridine type of ligands can be achieved through the few synthetic routes. Starting from the oligomeric $[\text{Ru}(\text{CO})_2\text{Cl}_2]_n$ one can consecutively introduce polypyridine ligands as shown in Scheme 1A to obtain $[\text{RuL}^1\text{L}^2\text{L}^3]^{2+}$ [33–37]. Noteworthy, in the last step, decarbonylation is induced with trimethylamine *N*-oxide (TMNO), which transfers oxygen resulting in CO_2 and TMA. Moreover, authors visually observed that the coordination of the last ligand L^3 is faster when L^1 and L^2 are more electron withdrawing, which increase the π -backbonding from the Ru $d\pi$ orbitals to L^1 and L^2 , and thus decreasing the Ru–CO bond order [37]. To the best of our knowledge, there is no reported synthesis of *tris*-heteroleptic ruthenium complexes with two *isothiocyanate* ligands through this synthetic route.



Scheme 1. Synthesis of *tris*-heteroleptic ruthenium complexes with polypyridine ligands. (A–C) represent routes starting from different sources of ruthenium. The scheme is build according to the published literature [35,38,39].

Zakeeruddin et al. introduced another way for synthesis of *tris*-heteroleptic ruthenium complexes, especially with isothiocyanate ligands [40]. As shown in Scheme 1B, starting from $\text{Ru}(\text{DMSO})_4\text{Cl}_2$ four DMSO ligands are substituted in two step to two different bipyridine type ligands. Then, in the last step, two chlorides are substituted with isothiocyanate ligands.

Tris-heteroleptic ruthenium complexes can also be obtained through the procedure developed by Freedman et al., in which $[\text{Ru}(\text{Bz})\text{Cl}_2]_2$ is used as a Ru source (Scheme 1C) [39]. In opposite to the aforementioned procedures, only mild reaction conditions are used in this route, which should prevent ligand scrambling and result in higher yields of *tris*-heteroleptic product. This procedure was further modified to synthesize *tris*-heteroleptic ruthenium complexes with isothiocyanate ligands in one-pot reaction. With this new procedure, Zakeeruddin et al. introduced Z907 sensitizer $\text{RuL}^1\text{L}^2(\text{NCS})_2$ where L^1 is 4,4'-dicarboxy-2,2'-bipyridine, and L^2 is 2,2'-bipyridine derivatized on 4 and 4' th positions with nonyl chains [38]. The gained hydrophobicity should protect oxide-electrolyte interface from water and thus prevent water induced dye desorption. Although in reference to N749, Z907 showed lower PCE of 6.2%, the stability of device with Z907 was significantly improved [41]. Moreover, gelation of 3-methoxypropionitrile electrolyte solution with a polymer resulted in improved stability. Z907 sensitizer set a precedent for hundreds of *tris*-heteroleptic ruthenium complexes with isothiocyanate ligands that were developed in the last fifteen years. However, these new sensitizers rarely provided efficiencies comparable to the N719, making the set direction in DSCs research questionable.

Many analogues of Z907 with different substituents on the 4 and 4' positions of auxiliary 2,2'-bipyridine ligand were tested. Most popular among them are complexes with substituents based on styrol, thiophen, and triphenyl amine. The need for the high-extinction coefficient dyes was the main

cause for this shift toward the *tris*-heteroleptic complexes with various aromatic substituents. In a new Z910 complex the nonyl chains on the ancillary ligand of Z907 were substituted with 3-methoxystyryl moieties [42]. In the result, the MLCT absorption bands of Z910 reached extinction coefficients of 16.85×10^3 and 17×10^3 ($\text{M}\cdot\text{cm}$)⁻¹. In a DSC of conventional architecture, Z910 provided PCE of 10.2% with J_{SC} and V_{OC} reaching $17.2 \text{ mA}\cdot\text{cm}^{-2}$ and 777 mV, respectively. Afterwards, sensitizers K19 and K77, differing from Z910 by the position and length of the alkoxy groups were introduced [43–45]. However, these sensitizers showed lower efficiencies than Z910. Moreover, N719 sensitized solar cell of unexpectedly low 6.7% efficiency was used as a reference.

The *tris*-heteroleptic isothiocyanate ligated ruthenium complexes with different thiophene-based substituents are shown in Figure 6. All of these sensitizers have aromatic moieties on the ancillary ligand with additional alkyl chains. The main purpose of adding these aromatic moieties is to increase the absorptivity of sensitizer. Alkyl chains are introduced for two reasons: to increase the solubility of sensitizer and to prevent dye-aggregation on titania surface. One would expect that sensitizers with more complex substituents would be reported later in history, which is not the case. CYC-B1 sensitizer with 2,2'-bithiophene substituents with additional octyl chains on the 5' positions of each thiophene was reported by Chen et al. [46]. The absorption spectrum of CYC-B1 reveals two apparent bands in the visible region with absorption maxima at ca. 400 and 553 nm and with extinction coefficients of ca. 46.4×10^3 and 20×10^3 ($\text{M}\cdot\text{cm}$)⁻¹. A DSC with CYC-B1 provided J_{SC} of $24 \text{ mA}\cdot\text{cm}^{-2}$ and V_{OC} of 650 mV, however, low FF of 55% limited PCE to only 8.54%, which is 10% higher than the reference device with N3 sensitizer. From the shape of the *J-V* curve, one might suspect that low FF is result of increased device series resistance, which is reasonable considering that a titania film of 20 μm was used and that the distance between two electrodes was 80 μm . Afterwards, the same authors introduced CYC-B3 and CJW-E1 with 5-octyl-thiophene and 5-octyl-EDOT (EDOT—3,4-ethylenedioxythiophene) substituents on the ancillary ligand respectively [47]. According to this work, the extinction coefficient of the lowest energy MLCT band for CYC-B3 differ negligibly from that of N3. Although the absorption spectra of CYC-B3 and CJW-E1 are very close, DSC with former provided PCE of 7.39%, while with latter—PCE of 9.02%. DSC on CJW-E1 gave J_{SC} of $21.6 \text{ mA}\cdot\text{cm}^{-2}$ and on CYC-B3—only $15.7 \text{ mA}\cdot\text{cm}^{-2}$, with both devices providing the same V_{OC} of 669 mV. Authors did not provide any reasonable explanation behind PCE differences. Surprisingly, a monodeprotonated analogue of CYC-B3 with shorter alkyl chains C101, was also studied, and high PCE of 11% was achieved [48]. In another work, the analogue of CJW-E1, C103 with just hexyl-chains on the EDOT and in a monodeprotonated form, was shown to provide a PCE of 10.4% [49]. This disagreements in results obtained with very similar sensitizers in different laboratories undermine the general logic of sensitizer design and the validity of discussion behind the obtained results.

Some reports also show that substitution of alkyl chains in C101 and CYC-B1 by thioalkyl chains results in better performing sensitizers C106 and CYC-B11 [50,51]. However, the positive effect of this modification can be questioned. For example, the performances of C106 and C101 were compared, where these sensitizers provide PCEs of 10.57% and 10.33% respectively. Based on merely 0.2% PCE difference, C106 was chosen and its performance was optimized with better films to reach the PCE of 11.29% [50]. However, the same authors one year earlier published 11.0% PCE with C101 [48]. Thus, the advantage of introducing thioalkyl chains instead of simple alkyl chains is not valid yet.

Another group of *tris*-heteroleptic ruthenium complexes with two isothiocyanate ligands are those with arylamine-based electron donors attached at the ancillary ligand. Electron rich substituents were introduced to increase π -conjugation on the ancillary ligand and destabilize the ground state oxidation potential and HOMO through π -donation. Such design should lead to high and panchromatic molar absorptivity. Moreover, electron rich arylamine donors should enable efficient hole extraction and thus facilitate dye-regeneration with solid-state devices, employing hole-transporting materials like Spiro-OMeTAD [52]. Some of the *tris*-heteroleptic ruthenium complexes with arylamine electron donors are presented in Figure 7 and their performances are summarized in Table 1. As one may notice, these additional complications of dye structure did not lead to any substantial improvements in

device performance. The general note regarding most of these articles on *tris*-heteroleptic ruthenium complexes with isothiocyanate ligands is that they usually report one or two new sensitizers with some random aromatic moiety, and very rarely performances of a series of few sensitizers are compared.

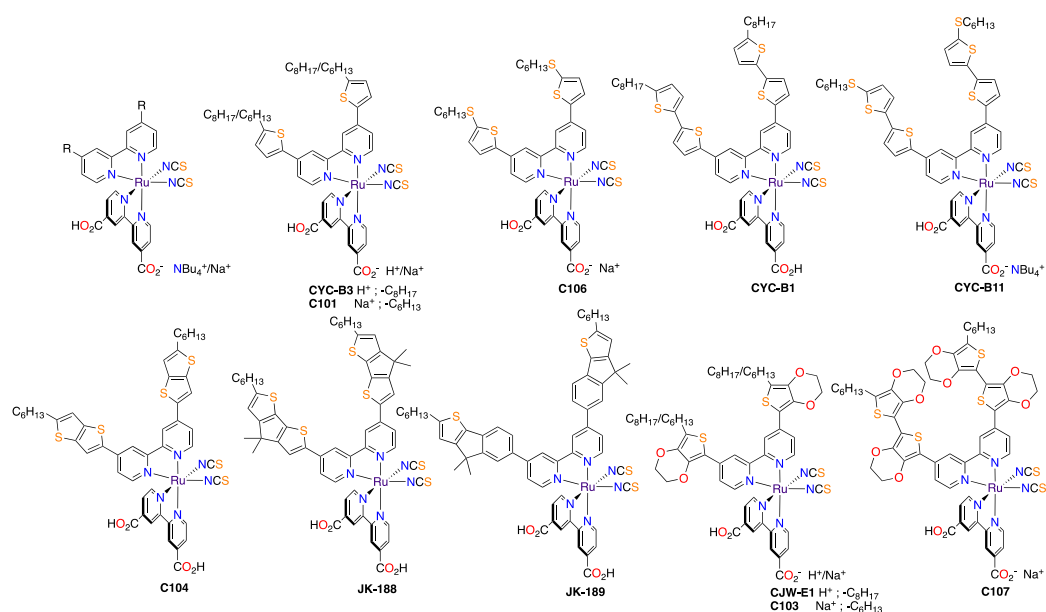


Figure 6. Some of the *tris*-heteroleptic isothiocyanate ligated Ru(II) complexes with thiophene-based substituents on the ancillary ligand.

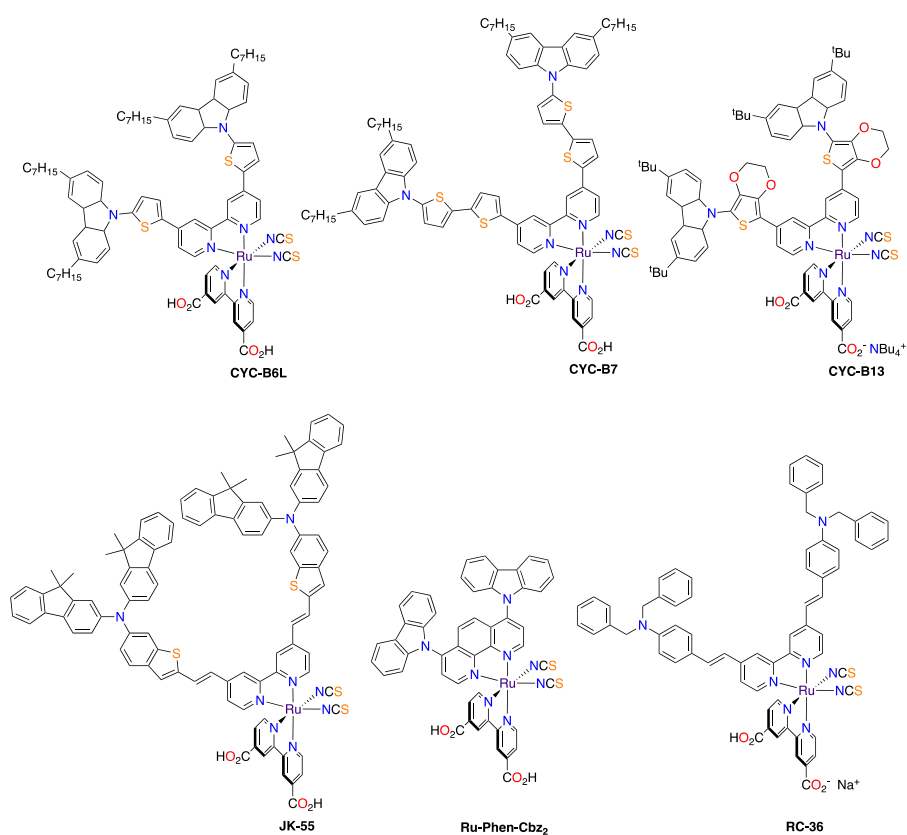


Figure 7. Some of the *tris*-heteroleptic isothiocyanate ligated Ru(II) complexes with arylamine-based substituents on the ancillary ligand.

Table 1. Performances of selected *tris*-heteroleptic ruthenium complexes with isothiocyanate ligands and with thiophene-based substituents on the ancillary ligand.

Groups ^a	Dye	J_{SC} , mA·cm ⁻²	V_{OC} , mV	FF, %	PCE, %	Notes ^b
NTU	CYC-B1	23.92	650	55.0	8.54	20 μm thick mesoporous film; 80 μm between electrodes [46,47].
	CYC-B3	15.7	669	70.5	7.39	
	CJW-E1	21.6	669	62.6	9.02	
CIAC & EPFL	C101	17.94	777.7	78.5	11.0	7 μm of transparent TiO ₂ + 5 μm scattering TiO ₂ ; dipping solution: Dye-Cheno [48].
CIAC	C103	18.35	760	74.8	10.4	7.5 μm of transparent TiO ₂ + 5 μm scattering TiO ₂ [49].
	C107	19.18	739	75.1	10.7	
CIAC & EPFL	C104	17.87	760	77.6	10.53	7 μm of transparent TiO ₂ + 4 μm scattering TiO ₂ ; dipping solution: Dye-Cheno (1–1) [53].
KU	JK-188	18.60	720	71	9.54	10 μm of transparent TiO ₂ + 4 μm scattering TiO ₂ [54].
	JK-189	18.90	630	73	8.70	
NCU & EPFL	CYC-B11	18.3	704	73	9.4	8 μm of transparent TiO ₂ + 5 μm scattering TiO ₂ ; dipping solution: Dye-DINHOP (4–1) [51].
CIAC	C106	19.2	776	76	11.29	7 μm of transparent TiO ₂ + 5 μm scattering TiO ₂ ; dipping solution: Dye-Cheno (1–6.7) [50].
NCU	CYC-B6L	18.2	776	63.6	8.98	15 μm thick mesoporous film; 80 μm between electrodes [55].
NTU & NCU	CYC-B7	17.4	788	65.4	8.96	15 μm thick mesoporous film; 80 μm between electrodes [56].
NCU & EPFL	CYC-B13	10.26	728	68	5.1	8 μm of transparent TiO ₂ + 5 μm scattering TiO ₂ [57].
KU & EPFL	JK-55	17.55	640	72	8.2	10 μm of transparent TiO ₂ + 4 μm scattering TiO ₂ ; dipping solution: Dye-Cheno (1–3.3) [58].
UFABC	Ru-Phen-Cbz2	15.6	760	71.6	8.5	13 μm thick mesoporous film; 30 μm between electrodes [59].
HIPS	RC-36	19.17	721	74	10.23	4 μm of transparent TiO ₂ + 16 μm scattering TiO ₂ ; dipping solution: Dye-DPA (2–1) [60].

^a NTU—National Taiwan University, Taiwan; EPFL—École Polytechnique Fédérale de Lausanne, Switzerland; CIAC—Changchun Institute of Applied Chemistry, China; KU—Korea University, Korea; NCU—National Central University, Taiwan; UFABC—Universidade Federal do ABC, Brazil; HIPS—Hefei Institutes of Physical Sciences;

^b Cheno—3α,7α-dihydroxy-5β-cholic acid; DINHOP—dineohexyl phosphinic acid; DPA—1-decylphosphonic acid.

Many analogues of above mentioned N749 or black dye were also studied. In these complexes, ruthenium is usually coordinated with three isothiocyanate ligands and one tridentate ligand based on 2,2':6',2''-terpyridine. The most convenient route to synthesize black dye and its derivatives consists of two steps. First, RuCl₃·xH₂O is reacted with the tridentate ligand L to obtain RuLCl₃, which, due to their low solubility in most of the solvents, are difficult to characterize, and usually subjected to the second step to substitute chlorides with isothiocyanates.

In a search for a better sensitizer than N749, its anchoring ligand was modified. In Figure 8, two main possibilities of anchoring ligand modification are represented. In Figure 8A some of the tested alternatives are shown. Presented sensitizers either suffer from blueshifted absorption spectra [61,62], or from inefficient charge injection due to low energy of excited states, thus resulting in poor power conversion efficiencies [63–65]. Alternatively, one of the terminal pyridine rings of N749 was modified to improve the photophysical characteristics of sensitizer. In Figure 8B, some of the well-performing sensitizers are presented. Insertion of electron donating substituents on the fifth position of terminal pyridine ring does not result in increased extinction coefficient for the lowest

energy MLCT band. However, between 350 and 550 nm, the absorption spectrum intensity strongly increases. This substitution also results in a small cathodic shift of oxidation potential, which should not influence dye-regeneration efficiency. Although the reference cell employing black dye provided PCE of only 6.89%, all three sensitizers PRT-12, PRT-13, and PRT-14 provide much higher PCE of 9.1%, 10.3%, and 8.86% respectively (Table 2) [66]. The improved performance of device with PRT-13 having EDOT moiety is related to both: higher J_{SC} and V_{OC} than with other sensitizers. Electrochemical impedance spectroscopy analyses revealed that the electron lifetime in devices with PRT-13 is higher than with other sensitizers leading to 760 mV V_{OC} . Higher J_{SC} achieved with PRT-13 than with N749 or with PRT-14, is surprising (16.8, 19.7, and 17.8 $\text{mA}\cdot\text{cm}^{-2}$ for N749, PRT-13, and PRT-14 respectively), and we believe it is the result of compromise between dye-loading and the absorption spectrum intensity. Due to its size, more PRT-13 should load onto titania than PRT-14 and less than N749. Although authors did not investigate it directly, this work underlines the role of dye-loading.

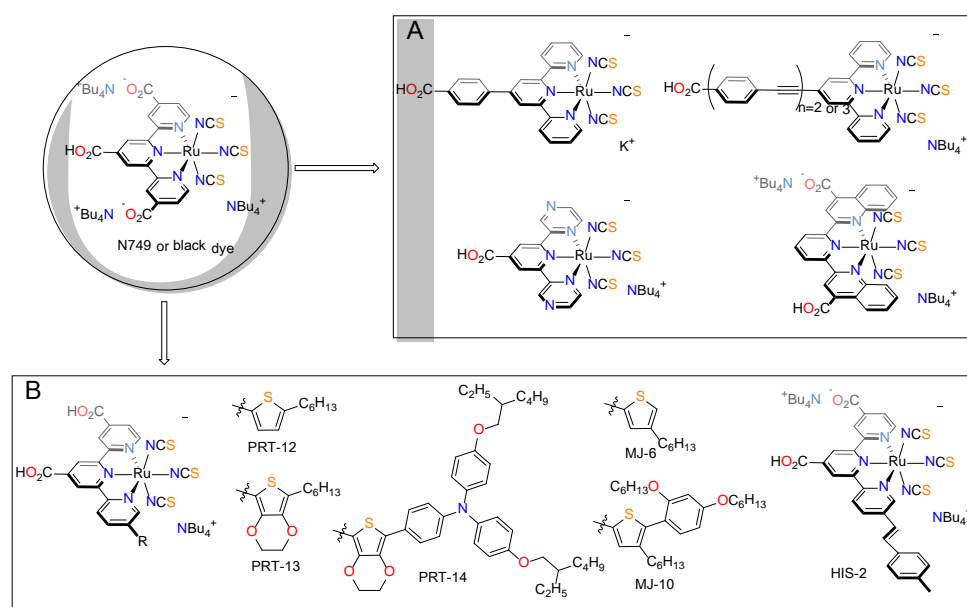


Figure 8. Black dye, and two popular directions to modify tridentate ligand. (A,B) represent two different ways to modify the N749.

Table 2. Performance of selected ruthenium complexes with tridentate accepting ligand and three isothiocyanate donating ligands.

Groups ^a	Dye	J_{SC} , $\text{mA}\cdot\text{cm}^{-2}$	V_{OC} , mV	FF, %	PCE, %	Notes ^b
NTHU & NTU	PRT-12	17	750	71.5	9.1	15 μm of transparent TiO_2 + 5 μm scattering TiO_2 ; dipping solution: Dye-Cheno (1–33); PCE with N749—6.89% [66].
	PRT-13	19.7	760	68.6	10.3	
	PRT-14	17.8	720	69.0	8.86	
SU & AIST	MJ-6	18.1	680	71	8.7	14 μm of transparent TiO_2 + 7 μm scattering TiO_2 ; dipping solution: Dye-Cheno (1–100); PCE with N749—9.2% [67].
	MJ-10	18.3	690	72	9.1	
NIMS & UT	HIS-2	23.07	680	71	11.1	25 μm thick mesoporous layer; 40 μm between electrodes; dipping solution: Dye-Cheno (1–67); PCE with N749—10.5% was obtained [68].

^a NTHU—National Tsing Hua University Taiwan; NTU—National Taiwan University; SU—Shinshu University, Japan; AIST—National Institute of Advanced Industrial Science and Technology; NIMS—National Institute for Material Science, Japan; UT—University of Toyama, Japan.

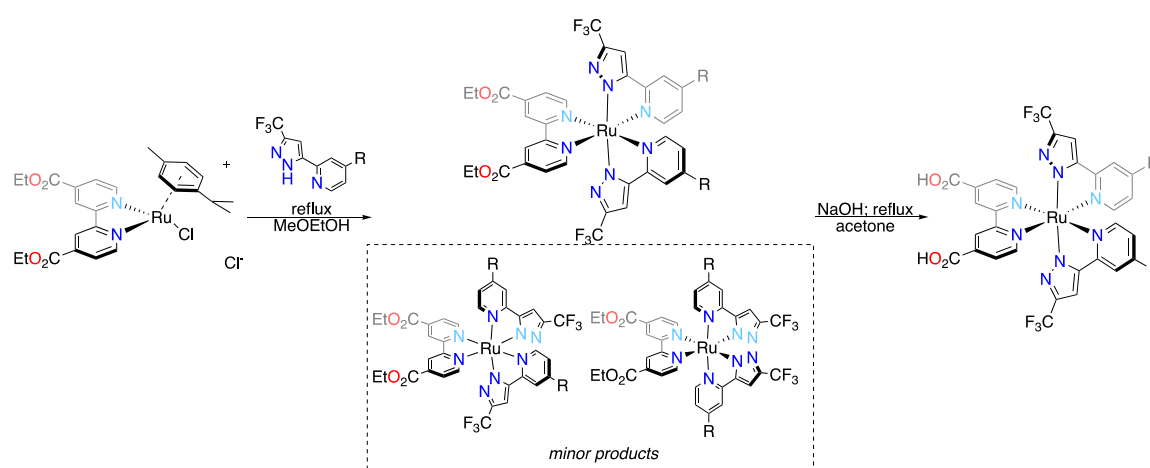
In another work, with analogous sensitizers—MJ-6 and MJ-10, high PCEs were achieved (Table 2) [67]. More intense absorption band of MJ-6 and MJ-10 in near UV-region of visible light results in improved IPCE. However, better absorption of N749 at low energies resulted in higher obtained

J_{SC} of $19.0 \text{ mA}\cdot\text{cm}^{-2}$ with N749 than with MJ-6 and MJ-10, which gave 18.1 and $18.3 \text{ mA}\cdot\text{cm}^{-2}$ respectively. Impressive result was achieved with HIS-2 with 4-methylstyryl moiety attached onto the terminal pyridine ring [68]. It worth noting, that in opposite to PRT and MJ series of sensitizers mentioned above, authors isolated HIS-2 in its monodeprotonated form. In comparison to N749, HIS-2 exhibits improved absorption spectrum through the whole visible region, and thus in higher IPCE. Solar cells with $25 \mu\text{m}$ thick mesoporous layer with HIS-2 provided impressive $23.07 \text{ mA}\cdot\text{cm}^{-2}$ J_{SC} , and PCE of 11.1%. As a reference, N749 provided J_{SC} and PCE of $21.28 \text{ mA}\cdot\text{cm}^{-2}$ and 10.5%. Both devices had close V_{OC} of 680 and 690 mV, which indicates that PCE improvement is solely due to improved light absorption.

3.2. Toward Isothiocyanate Free Ruthenium Complexes

As a monodentate ligand, isothiocyanates are labile under thermal or light stress. Standard electrolytes employed in DSCs contain iodide anions or 4-*tert*-butylpyridine in high concentrations, which further favors isothiocyanate substitution [69–71]. To obtain kinetically inert sensitizers, isothiocyanate free ruthenium complexes with bi- or tridentate donating ligands were developed [72–76].

Prof. Yun Chi's and Prof. Pi-Tai Chou's groups have extensively studied ruthenium complexes with 1,2-pyrazolyl and 1,2,4-triazolyl ligands. The standard bidentate ligand frequently used is 2-(3-(trifluoromethyl)-1H-pyrazol-5-yl)pyridine illustrated in Scheme 2. This ligand binds to ruthenium in a deprotonated form, thus a charge neutral ruthenium complexes with two pyridine-pyrazolyl ligands and one 4,4'-dicarboxy-2,2'-bipyridine ligand [$\text{Ru}(\text{PyPz})_2(\text{bpy})$] can be obtained [77–79]. These new type of sensitizers are synthesized in three steps starting from [$\text{Ru}(\text{p-Cymene})\text{Cl}_2$] $_2$ as illustrated in Scheme 2. First, [$\text{Ru}(\text{p-Cymene})\text{Cl}_2$] $_2$ is reacted with 4,4'-dicarboxy-2,2'-bipyridine diethyl or dimethyl ester (bpy') and [$\text{Ru}(\text{bpy}')(\text{p-Cymene})\text{Cl}$] Cl is obtained, which is then reacted with pyridine-pyrazolyl type of ligand in 2-methoxyethanol to obtain ruthenium complexes of three different coordination isomers. However, the isomer in which two pyrazolyl ligands are in *trans*-position to each other is the major product. This complex can be isolated via column chromatography and hydrolyzed to obtain the final complex with two carboxylic groups. However, the option of further isomerization during the last saponification step was not addressed.



Scheme 2. Synthesis of TFRS sensitizers with bidentate ligands.

In Figure 9 some of the well performing TFRS series sensitizers with bidentate pyridine-pyrazolyl type of ligands are presented. TFRS-1 with no substituents on the pyridine rings of pyridine-pyrazolyl ligand has a less intense absorption spectrum than N719. The lowest energy MLCT band of TFRS-1 has an extinction coefficient of $7900 \text{ (M}\cdot\text{cm)}^{-1}$, which is almost twice lower than that of N719 [77]. Introduction of 5-hexylthiophene or 5-hexyl-2,2'-bithiophene onto the 4th position of each pyridine in

TFRS-2 and TFRS-3 respectively has a hypsochromic effect on the absorption spectra of these sensitizers. Solar cells with 12 μm thick transparent mesoporous and 4 μm scattering layer employing TFRS-1, TFRS-2, and TFRS-3 were analyzed. Moving from TFRS-1 to TFRS-2, improved light absorption results in increased J_{SC} , while further from TFRS-2 to TFRS-3, enhancement of J_{SC} is negligible. On the other hand, in the same line, V_{OC} drops from 830 for TFRS-1 to 820 and 810 mV for TFRS-2 and TFRS-3 respectively. In the result TFRS-1, TFRS-2, and TFRS-3 provide PCEs of 9.18%, 9.54%, and 8.94% respectively. Via electrochemical impedance spectroscopy analysis of devices, authors showed that moving from TFRS-1 to TFRS-2, and TFRS-3 the recombination resistance in devices drops, which explains the observed trend in V_{OC} . Authors illustrated that the absorbance of the mesoporous film sensitized with TFRS-3 is at least 20% higher than that sensitized with TFRS-2, which considering the obtained J_{SC} (Table 3) underlines very inefficient charge collection for the films with TFRS-3.

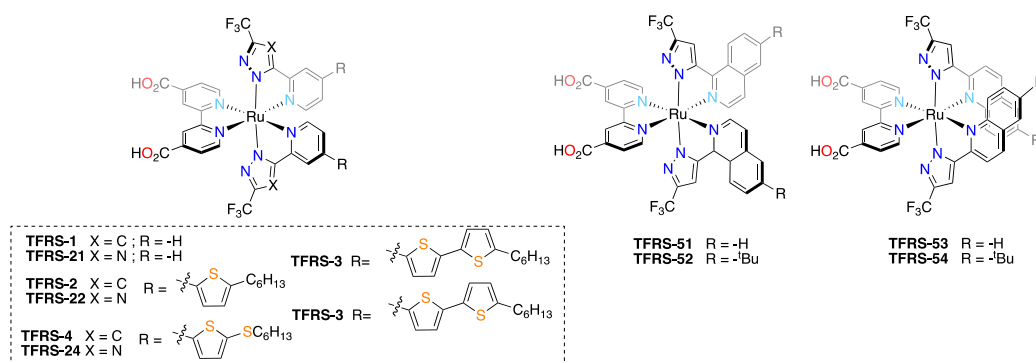


Figure 9. Some of the TFRS series sensitizers with bidentate ligands.

Table 3. Photovoltaic performance of selected TFRS series sensitizers with bidentate ligands.

Groups ^a	Dye	J_{SC} , $\text{mA}\cdot\text{cm}^{-2}$	V_{OC} , mV	FF, %	PCE, %	Notes
NTHU	TFRS-1	15.95	830	69.3	9.18	12 μm of transparent TiO_2 + 4 μm scattering TiO_2 ; PCE with N719—8.56% [77].
	TFRS-2	17.15	820	67.8	9.54	
	TFRS-3	17.38	810	63.5	8.94	
NTHU & EPFL	TFRS-4	18.7	750	72.9	10.2	12 μm of transparent TiO_2 + 6 μm scattering TiO_2 ; PCE with N719—9.52%, with TFRS-1 and TFRS-2—8.66% and 9.63% [78].
	TFRS-21	14.1	790	69.5	7.74	
	TFRS-22	15.4	740	72.8	8.30	
NTHU, EPFL & NTU	TFRS-24	15.5	720	73.9	8.25	
	TFRS-51	15.4	760	75	8.80	12 μm of transparent TiO_2 + 6 μm scattering TiO_2 ; pce with TFRS-1—7.84% [79].
	TFRS-52 ^b	16.3/16.8	860/832	72/78	10.1/10.88	
	TFRS-53	14.6	780	73	8.36	
TFRS-54	14.7	860	71	8.94		

^a NTHU—National Tsing Hua University; EPFL—École Polytechnique Fédérale Lausanne; NTU—National Taiwan University; ^b Devices were prepared in two different institutes NTHU/EPFL.

Later, TFRS-4 with 5-thiohexylthiophene moieties attached onto the pyridine ring of pyridine-pyrazolyl ligand was introduced. Moreover, analogues of TFRS-1, TFRS-2, and TFRS-3 in which pyrazolyl ring is substituted to triazolyl—TFRS-21, TFRS-22, and TFRS-24 respectively, were introduced [78]. Among the newly presented sensitizers, TFRS-4 provided an exceptionally high PCE of 10.2%, while the reference device with N719—9.52% efficiency was achieved. In comparison to sensitizers with pyrazolyl moiety, those with triazolyl moiety presented narrower, more blueshifted, and less intense MLCT bands in the visible range. The more blueshifted MLCT bands in TFRS-21, TFRS-22, and TFRS-24 in comparison to TFRS-1, is the consequence of triazole being more electron withdrawing than pyrazole, which stabilizes occupied frontier molecular orbitals. The same conclusion is supported with cyclic voltammetry measurements, which shows that moving from pyrazolyl to triazolyl ligated complexes the ground state oxidation potential is anodically shifted by 150–250 mV,

from ca. 0.9 to 1.1 V vs. NHE. A similar shift is estimated for the excited state oxidation potential. Regarding PCE in solar cells, sensitizers with triazolyl moiety show in average 1–2% lower efficiencies in comparison to those with pyrazolyl, which is due to both lower voltages and photocurrents.

In the following work, new TFRS complexes with isoquinoline and quinoline instead of pyridine in pyridine-pyrazolyl ligand—TFRS-51 and TFRS-53 respectively, were introduced (Figure 9) [79]. For both of these complexes derivatives with *tert*-butyl group on the 6th position of quinoline and isoquinoline, TFRS-52 and TFRS-54 respectively, were also prepared. Although the lowest energy absorption band for these new series of sensitizers with quinoline and isoquinoline moieties are by 15–20 nm more blueshifted than that for TFRS-1, higher extinction coefficient for TFRS-51, TFRS-52, TFRS-53, and TFRS-54 result in better visible light harvesting. Interestingly, sensitizers with quinoline moiety TFRS-53 and TFRS-54 have less intense absorption spectra than that with isoquinoline TFRS-51 and TFRS-52. In solar cells new sensitizers exhibit better performance in comparison to TFRS-1. However, it worth noting that in this work PCE of 7.84% with TFRS-1 as the reference was reported, while in the previous work with the same sensitizer 9.18% conversion efficiency was achieved. Nevertheless, TFRS-52 with 6-*tert*-butylisoquinoline moiety provided a PCE of 10.1% mostly due to high V_{OC} reaching 860 mV. The same TFRS-52 tested at EPFL provided 10.88% conversion efficiency as better FF and J_{SC} , with little lower V_{OC} were obtained [79]. Authors explained the variation in PCEs on the basis of electron lifetime and conduction band edge shifts. In comparison to TFRS-51 and TFRS-53, sensitizers with additional *tert*-butyl group (TFRS-52 and TFRS-54) result in upward shift of the conduction band edge and in higher recombination resistances. Interesting to note that TFRS series sensitizers with bidentate ligands in devices with iodine-based electrolyte provide surprisingly high V_{OC} of over 800 mV. Such a high V_{OC} was before achieved with fully deprotonated N3 sensitizer. To investigate reasons behind comparatively high V_{OC} achieved with TFRS series complexes, Moehl et al. analyzed solar cells with TFRS-2, Z907, and C101 [80]. First, standard solar cells were fabricated and better performance with TFRS-2 than with Z907 and C101 was obtained, as a result of both higher J_{SC} and V_{OC} achieved with TFRS-2. Higher J_{SC} obtained with TFRS-2 can be related on the one side to its broader and more intense absorption spectrum in comparison to Z907 and C101, and on the other side, to the higher dye-loading obtained with TFRS-2 than with Z907 and C101 sensitizers. According to the electrochemical impedance spectroscopy analysis, both, improved charge recombination resistance and upward shift of the conduction band edge are responsible for higher V_{OC} obtained with TFRS-2 than Z907 and C101 sensitized solar cells. With the means of DFT calculations, the shift of the conduction band edge was related to the dye dipole moment directed away from the surface in case of TFRS-2. In contrast, for solar cells sensitized with Z907 and C101, due to the partial negative charge on the isothiocyanate ligands, molecule's dipole moment is directed toward the surface (Figure 10).

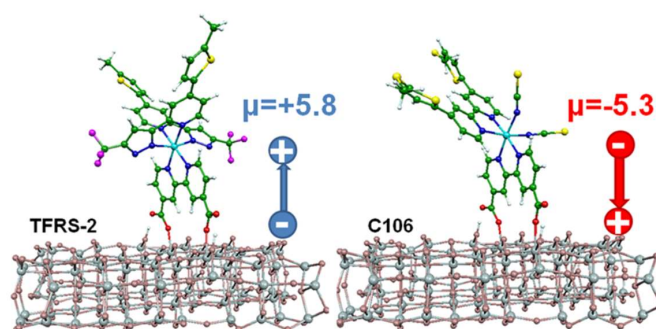


Figure 10. Optimized geometries of TFRS-2 and C101 along with the calculated dipole moments of the neutral dyes at their adsorption geometries. Alkyl chains have been replaced by methyl group. Reprinted with permission from *Chem. Mater.* 2013, 25, 4497–4502 [80]. Copyright (2013) American Chemical Society.

Analogues of above-mentioned TFRS sensitizers, but derived from N749 rather than N3 sensitizer, were also developed (Figure 11). Among them are PRT1–PRT4 complexes with one tridentate 4,4',4''-tricarboxy-2,2':4',2''-terpyridine, one functionalized bidentate pyridine-pyrazole, and with single isothiocyanate ligands [81]. In comparison to the N749, these new complexes possess broader absorption spectra with onset reaching 850 nm, and better absorptivity below 550 nm. The ground state oxidation potentials for these sensitizers adsorbed onto the mesoporous titania of ca. 0.6–0.7 V vs. NHE were measured via cyclic voltammetry. Interestingly, for PRT-1 with no substituents on the styryl group, lower oxidation potential of 0.6 V, while for PRT2, PRT3, PRT4 with methoxy, hexyloxy, and *tert*-butyl substituents on the styryl group, higher oxidation potentials in the range of 0.7–0.71 V vs. NHE were measured. Assembled solar cells with 6 μm mesoporous film and iodine-based electrolyte provided PCEs of 9.14–10.05% with better results moving from PRT1 to PRT4, while the reference solar cells with N749 provided 9.07% (Table 4). After these promising results, another series of PRT sensitizers, namely PRT21–PRT24 with two different tridentate anchoring and two pyrazolyl-pyridine ligands were reported (Figure 11) [82]. Anchoring ligands were 4,4',4''-tricarboxy-2,2':4',2''-terpyridine and its derivative where one of the terminal pyridines is substituted by 6-*tert*-butylquinolin-8-yl (Qbpy). Two pyrazolyl-pyridine donor ligands have either 5-hexylthien-2-yl or 5-(hexylthio)thien-2-yl substituents at the 4th-position of the pyridyl ring. Complexes PRT22 and PRT24 with hexylthio-chain show more intense absorption spectra than their analogues PRT21 and PRT23 with just hexyl-chain. Additionally, complexes with Qbpy anchoring ligand, PRT23 and PRT24, exhibit broader absorption spectra with higher extinction coefficients at almost whole visible range than PRT21 and PRT22 with terpyridine anchoring ligand. However, a 6- μm thick mesoporous layer of titania sensitized with PRT21 and PRT22 showed more intense absorption spectra than those with PRT23 and PRT24. This outcome can be related to higher dye-loading obtained with PRT21 and PRT22. For all four sensitizers, assembled solar cells with a 15- μm thick transparent and a 7- μm thick scattering layer of mesoporous titania provided efficiencies higher than the reference cell with N749 dye. Interestingly, devices with PRT22 and PRT24 possessing hexylthio-chain provide consistently higher J_{SC} and lower V_{OC} than devices with PRT21 and PRT23 having a simple hexyl chain. In the result, sensitizers PRT22 and PRT24 provided little higher PCEs than PRT21 and PRT23—11.16% and 10.51% vs. 10.81% and 10.43% (Table 4). Higher currents obtained with PRT22 and PRT24 than with PRT21 and PRT23, were explained as a result of differences in absorption spectra. However, the explanation behind the obtained voltages was not straightforward, considering that different sensitizers provided different conduction band edge positions, various electron lifetimes, and various dye-loadings, with no clear correlations of each factor with structural modifications.

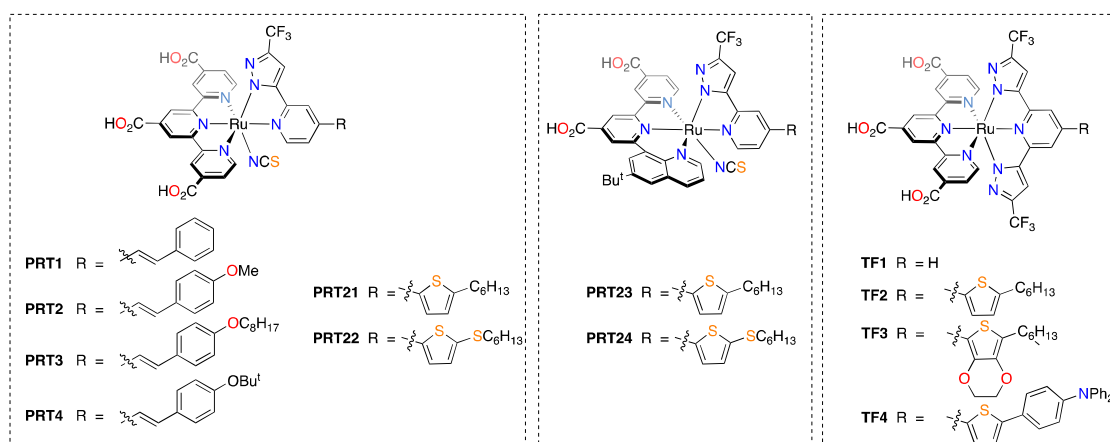


Figure 11. Selected PRT and TF series sensitizers with bidentate and tridentate ligands.

Table 4. Photovoltaic performance of selected PRT and TF series sensitizers with bidentate and tridentate ligands.

Groups ^a	Dye	J_{SC} , mA·cm ⁻²	V_{OC} , mV	FF, %	PCE, %	Notes
NTU & NTHU	PRT1	20.3	687	65.4	9.14	18 μm of transparent TiO ₂ + 4 μm scattering TiO ₂ ; PCE with N749—9.07% [81].
	PRT2	21.7	668	64.4	9.33	
	PRT3	20.4	720	65.3	9.59	
	PRT4	21.6	714	65.2	10.05	
	PRT21	19.0	760	74.9	10.81	15 μm of transparent TiO ₂ + 7 μm scattering TiO ₂ ; PCE with N749—9.20% [82].
	PRT22	20.4	740	73.9	11.16	
	PRT23	18.7	760	73.4	10.43	
	PRT24	20.1	730	71.6	10.51	
NTHU, NTU & NCCU	TF1	18.22	740	67.6	9.11	15 μm of transparent TiO ₂ + 5 μm scattering TiO ₂ ; PCE with N749—9.22% [83].
	TF2	20.00	790	66.5	10.5	
	TF3	21.39	760	66.0	10.7	
	TF4	20.27	770	67.5	10.5	

^a NTHU—National Tsing Hua University (Taiwan); NTU—National Taiwan University (Taiwan); NCCU—National Chung Cheng University (Taiwan).

In further studies, analogues of PRT sensitizers with a tridentate-donating ligand based on 2,6-bis(5-pyrazolyl)pyridine were introduced. The main motivation in this shift was to improve the chemical stability and photophysical properties of new sensitizers. Initially, complexes TF1–TF4, where ruthenium is coordinated with tridentate terpyridine as an anchoring ligand and 2,6-bis(3-(trifluoromethyl)-1H-pyrazol-5-yl)pyridine or its derivatives with different electron donating substituents on the 4th position of pyridine ring were synthesized (Figure 11) [83]. Improved absorption spectra for TF1–TF4 sensitizers in comparison to N749 is questionable. These new sensitizers present more intense absorption bands than N749 at short wavelengths (below ca. 550 nm) and in near IR region, while less intense bands in-between. Solar cells with 15 μm thick transparent and 5 μm thick scattering layers of mesoporous titania, showed improved IPCE only below ca. 550 nm and around 700 nm for TF1–TF4 sensitizers than for N749 (Table 4). As a consequence, all new sensitizers apart TF1 provided higher J_{SC} than N749. In addition, crucial improvements in the V_{OC} resulted in PCEs over 10% for TF2–TF4 sensitizers, while 9.11 and 9.22 for TF1 and for the reference N749 sensitizers. Authors speculated that improved V_{OC} with TF sensitizers in comparison to N749 could be: (i) due to better packing of TF sensitizers resulting in increased recombination resistances, which was supported with electrochemical impedance spectroscopy analyses; and (ii) due to dipole moment in TF sensitizers directed toward the titania surface and pushing the conduction band edge upward. However, none of these claims were supported with analyses. Later, the same authors introduced new series of TF sensitizers where the anchoring ligand was modified. However, improvements in PCE were incremental and in some of the reports devices with new sensitizers were compared to the low-efficient references [84–86].

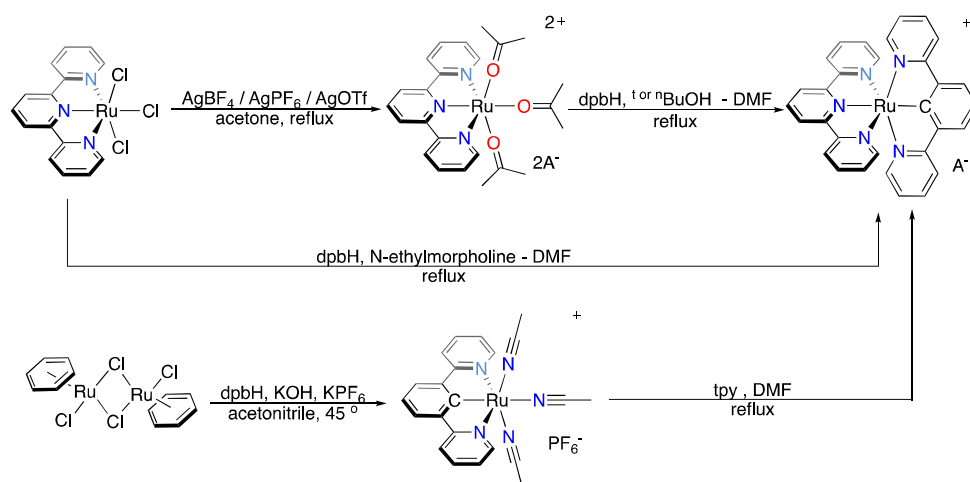
3.3. Cyclometalated Ruthenium(II) Complexes

After the first report on cyclometalated ruthenium complexes of $[\text{Ru}(\text{bpy})_2(\text{ppy})]^{1+}$ type (where ppyH = 2-phenylpyridine) by Reveco et al. [87–89] and by Constable with Holmes [90], these complexes attracted a great attention in regards their photophysical characteristics [91–97]. However, only in 2007 Wadman et al. reported on the potential of cyclometalated Ru(II) complexes for DSC application [98]. In comparison to $[\text{Ru}(\text{bpy})_3]^{2+}$ stronger electron donation from the carbanion in cyclometalated $[\text{Ru}(\text{bpy})_2(\text{ppy})]^{1+}$ results in higher electron density at Ru and in the upward shift of t_2 orbitals. In the result, cyclometalated ruthenium complexes present bathochromically shifted MLCT bands when compared to their imine coordinated analogues. According to the quantum mechanical calculations, three occupied frontier orbitals in cyclometalated Ru complexes, additional to the metal t_2 atomic orbital composition, have a significant contribution from the cyclometalated

ring's π^* orbitals [99]. This virtue provides the means to modify the occupied frontier orbital levels and thus tune the absorption spectrum and ground state oxidation potential by introducing various substituents onto the cyclometalating ligand. Another advantage with cyclometalated Ru complexes is the possibility to prepare *tris*-heteroleptic complexes where one can fine-tune photophysical properties of a complex modifying additional ligand. These complexes are analogous to the *tris*-heteroleptic Ru complexes with isothiocyanate ligands.

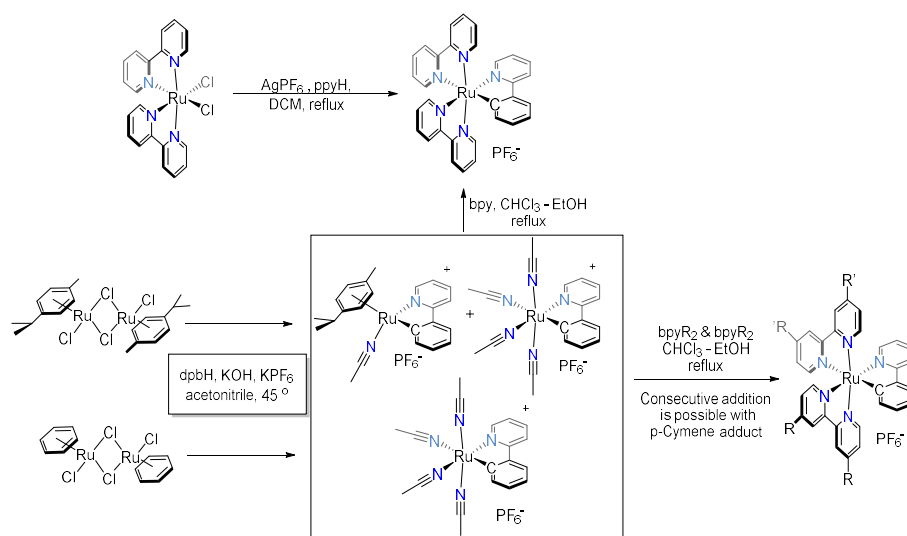
In their comprehensive studies, Bomben et al. presented a series of cyclometalated Ru complexes and compared them with noncyclometalated analogues. As the authors showed, cyclometalated complexes with broad absorption spectra and proper redox potentials are suitable for DSC application. Moreover, authors reported on convenient synthesis of both *bis*- and *tris*-heteroleptic cyclometalated ruthenium complexes.

To synthesize cyclometalated Ru complexes of $[\text{Ru}(\text{tpy})(\text{dpb})]^+$ type (where $\text{dpbH} = 1,3\text{-bis}(\text{pyridine-2-yl})\text{benzene}$) with two tridentate ligands, one may start from $\text{Ru}(\text{tpy})\text{Cl}_3$ and abstract halogens with soluble silver salts, i.e., AgPF_6 or AgBF_4 , in acetone, and then, without specific purification, react the obtained acetone ligated complex with a cyclometalating ligand as shown in Scheme 3 [94,96,100–104]. Direct reaction of $\text{Ru}(\text{tpy})\text{Cl}_3$ with cyclometalating ligand in the presence of base/reducing agent was also shown to provide cyclometalation [95,105–107]. Alternatively, one may start with $[\text{RuBzCl}_2]_2$ and react it first with a cyclometalating ligand in acetonitrile to obtain $[\text{Ru}(\text{dpb})(\text{CH}_3\text{CH}_2)_3]^+$, and then react the obtained complex with a polypyridine ligand [108–110]. Depending on the substituents on both, cyclometalating and polypyridine, ligands one may choose from the above-mentioned procedures.



Scheme 3. Synthesis of cyclometalated Ru-complex with two tridentate ligands.

Synthesis of *bis*-heteroleptic cyclometalated Ru complexes with bidentate ligands can also be achieved either by coordinating a cyclometalating ligand, like 2-phenylpyridine to $\text{Ru}(\text{bpy})_2\text{Cl}_2$ with or without the presence of silver salt [90,105,111], or more conveniently, through $[\text{Ru}(\text{ppy})(\text{CH}_3\text{CN})_4]^+$, in which the acetonitriles can be substituted with polypyridine ligands (Scheme 4) [112–115]. The latter route also provides means to synthesize *tris*-heteroleptic complexes where apart the cyclometalating ligand, two different bidentate polypyridine ligands are coordinated to ruthenium (Scheme 4) [113–117].



Scheme 4. Synthesis of cyclometalated Ru-complex with three bidentate ligands.

Bessho et al. showed that the simplest *bis*-heteroleptic cyclometalated Ru complex Bes1—[Ru(dcbpyH₂)₂(pF₂py)](PF₆), where HpF₂py is 2-(2,4-difluorophenyl)-pyridine—provides PCE over 10% (Figure 12) [111]. Authors present that in the final sensitizer used in solar cells all carboxylic groups are protonated, however reported ¹H and ¹³C NMR data support that the complex was obtained as a NBu₄⁺ salt, indicating that the complex is doubly deprotonated. Manufactured solar cells with 12 μm transparent and 5 μm scattering mesoporous titania provided 10.1% PCE, as 17 mA/cm² of J_{SC} and 800 mV of V_{OC} were obtained. In this work, the use of 2-phenylpyridine with two fluorines on the cyclometalating benzene ring was key to stabilize the ground state oxidation potential, and thus to favor photooxidized sensitizer regeneration. Afterwards, many cyclometalated *tris*-heteroleptic ruthenium complexes were introduced.

	Bes1	B1	B2
J _{sc} [mA/cm ²]	17.0	16.3	17.1
V _{oc} [mV]	800	660	630
FF [%]	74	68	67
PCE [%]	10.1	7.3	7.3

Figure 12. The photovoltaic performance of Bes1, B1, and B2 *tris*-heteroleptic cyclometalated ruthenium complexes. For Bes1 solar cells with transparent and scattering titania films of 12 and 3 μm thicknesses were manufactured [111]. B1 and B2 were reported in separated articles and highest efficiencies for both of them were achieved with the same electrolyte composition and with transparent and scattering titania films of 12 and 3 μm thicknesses [116,117].

Bomben et al. realized that substituting one of the 4,4'-dicarboxy-2,2'-bipyridine ligands with bpy leads to ca. 0.2 V cathodic shift of oxidation potential. To shift the oxidation potential back to 0.9–1.0 V vs. NHE, electron withdrawing substituents had to be introduced onto the cyclometalating ring. The effect of electron withdrawing substituents at cyclometalating and bpy ligands on the oxidation potential of ruthenium complexes is summarized in Figure 13 [118]. To improve the light harvesting ability cyclometalated complexes, aromatic substituent with alkyl chains were introduced at the ancillary bpy ligand. These substituents render sensitizer hydrophobicity, which should prevent water induced dye desorption and support device long-term stability. For example, sensitizer B1 with two 5-hexylthiophen-2-yl substituents on the ancillary ligand and 2-(2,6-bis-(trifluoromethyl)phenyl)pyridine as cyclometalating ligand provided PCE of 7.3%, while with the reference N3 sensitizer 6.3% PCE was achieved [116]. Although new sensitizer shows two-fold intense absorption spectrum than N3 sensitizer, due to compromise in dye-loading for B1 the absorbance of sensitized mesoporous films were not very different. The gain in efficiency was related to the improvement in J_{SC} from 13.3 mA/cm² for N3 to 16.3 mA/cm² for cyclometalating complex B1. According to the electrochemical impedance spectroscopy analyses, authors related the gain in J_{SC} to the improved charge recombination resistances (from 25 to 30 Ohm for N3 and B1). However, normalized diffusion lengths for both devices are much higher than the thickness of a mesoporous layer, which indicates that additional processes should be considered to fully explain the observed trend. In the follow-up article, the same group introduced a new sensitizer B2 with extended substituents on the ancillary ligand (Figure 12) [117]. Although solar cells with B2 provided higher J_{SC} than B1, the opposite is true for V_{OC} , resulting in comparable PCEs. Higher V_{OC} obtained with B1 than with B2 was again related to higher recombination resistance in devices with B1, which is not surprising as ca. 40% higher dye-loading was obtained with B1.

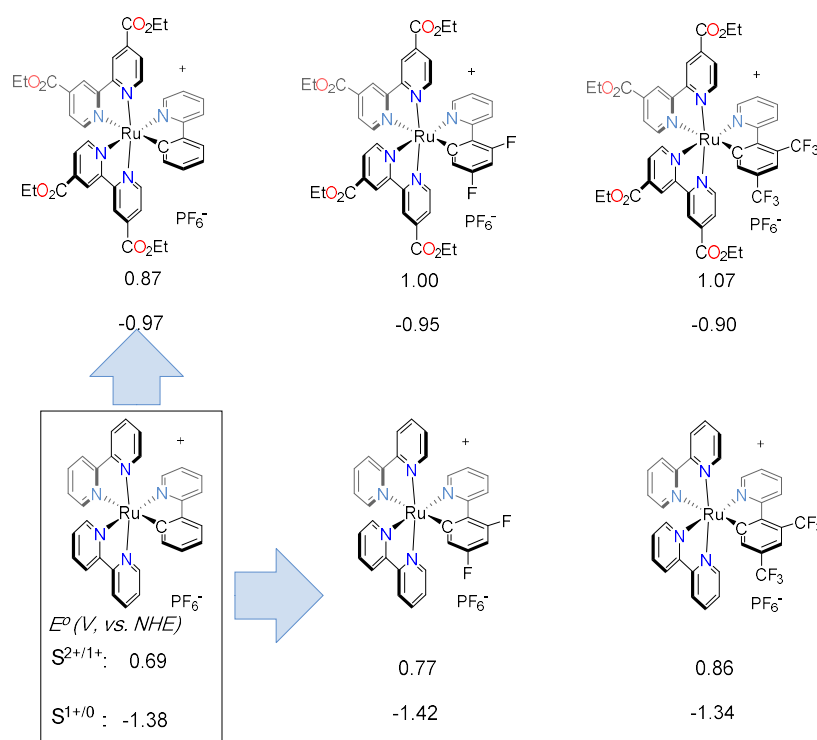


Figure 13. The change in first oxidation and reduction potential of cyclometalated ruthenium complexes upon introduction of electron-withdrawing substituents on both cyclometalating and bipyridine ligands. Oxidation potential values are taken from literature and were obtained in 0.1 M acetonitrile solution of LiClO₄ [118].

In the series of articles, Wadman et al. reported the synthesis and photophysical properties of *bis*-heteroleptic cyclometalated ruthenium complexes with tridentate ligands [94,95,98,99,108]. Especially, using symmetric NCN and asymmetric NNC ligands, authors underlined the effect of cyclometalated ring position on the photophysical properties of complexes [94]. Worth to notice that changing the NCN ligand to NNC results in a loss of degeneracy of HOMO-1 and HOMO-2 orbitals as the result of reduced symmetry from C_{2v} to C_i . Loss of degeneracy leads to additional mixed metal-ligand to ligand charge transitions. Generally, these *bis*-tridentate ruthenium complexes suffer from low extinction coefficients restricting their performance in solar cells [98]. To improve the absorption profile of these complexes, Robson et al. introduced various organic moieties at the cyclometalating ligand in a so called bichromic sensitizers [119,120]. Learning from the design principles for the organic donor- π -bridge-acceptor (D- π -A) sensitizers, authors introduced thiophene-bridge with triphenyl amine (TPA)-based organic electron donor at the 4th position of 6-phenyl-2,2'-bipyridine cyclometalating ligand. As illustrated in Figure 14, the choice of asymmetric 6-phenyl-2,2'-bipyridine over symmetric 1,3-bis(pyridine-2-yl)benzene cyclometalating ligand is crucial to observe donor-acceptor charge transfer. 2,2'-bipyridyl part of 6-phenyl-2,2'-bipyridine ligand plays a role of the charge acceptor.

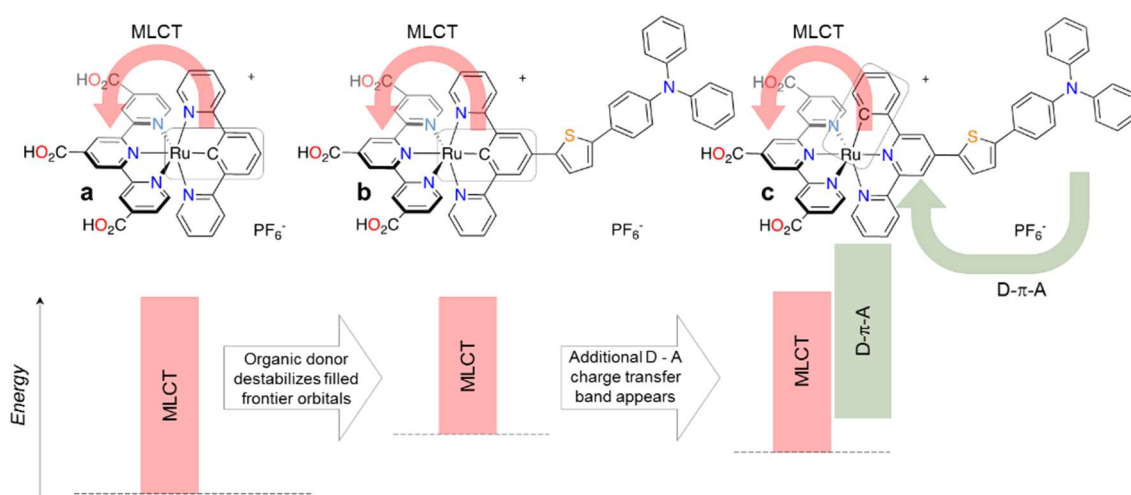


Figure 14. Design of bichromic sensitizers: moving from molecule **a** to **b** introduction of organic donor at the 1,3-bis(pyridine-2-yl)benzene (dpbH) cyclometalating ligand leads to destabilized filled frontier orbitals, and bathochromic shift of absorption spectrum. In case of molecule **c** with 6-phenyl-2,2'-bipyridine (pbpyH) cyclometalating ligand, additional D-A charge transfer band is appearing resulting in bichromic sensitizer.

Authors also showed that through modifications of either cyclometalating benzene ring or TPA moiety, an almost independent control over both $Ru^{3+/2+}$ and $TPA^{+/0}$ oxidation potentials is possible (Figure 15). For example, strong electron donating substituent, such as methoxy, at the TPA moiety, and electron withdrawing substituent, such as trifluoromethyl, at the cyclometalated ring, render TPA stronger reductant than Ru^{2+} . In the result, in the photooxidized sensitizer a TPA should extract a hole. It worth mentioning that ligands based on pbpy are less electron donating than those based on dpb as it is seen comparing $Ru^{3+/2+}$ oxidation potentials for complexes **b** and **c** from Figure 15.

The approach with bichromic sensitizers was fruitful. In a series of sensitizers with dpb and pbpy ligands, those with latter showed panchromatic absorption spectra and presented improved performance in the solar cells. Sensitizers A-Me and BC-Me, which have dpb and pbpy ligands respectively (Figure 16), provided PCEs of 3.90% and 6.33%. Moreover, modifying TPA with methoxy substituents in BC-OMe led to an even improved efficiency of 8.02%, while the reference cell with N3 sensitizer provided 8.65%. Interestingly, the bichromic sensitizer BC-H with no substituents

provided lower performance than BC-Me with methyl substituents on the TPA moiety, with no clear yet reason [107].

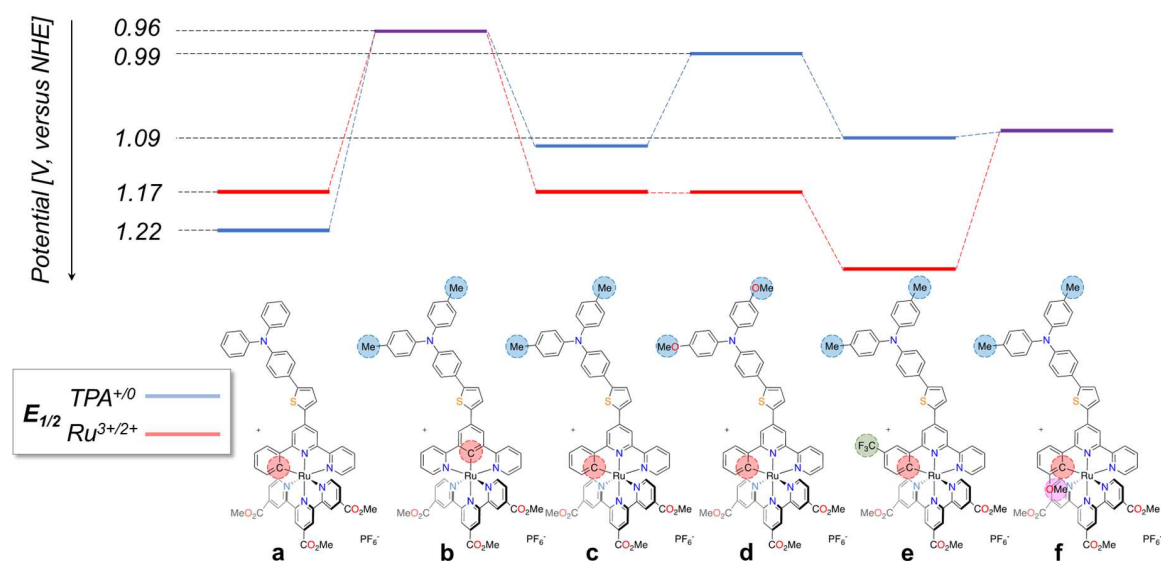
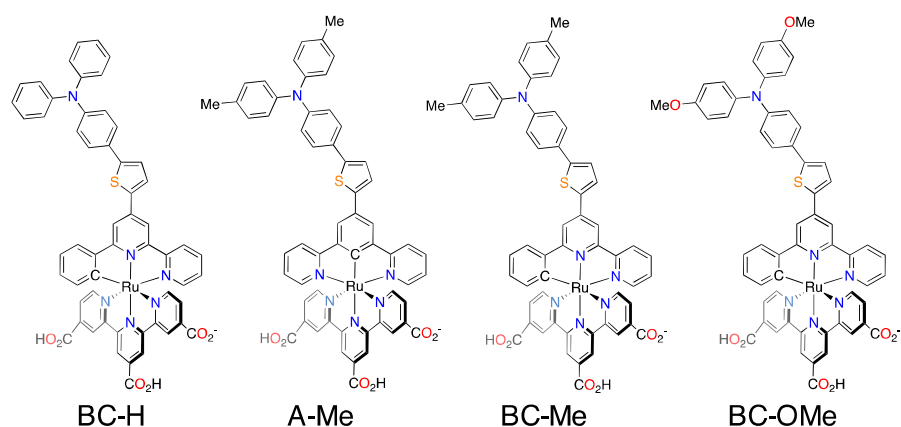


Figure 15. Control over $\text{Ru}^{3+/2+}$ and $\text{TPA}^{+/0}$ oxidation potentials. Upon introduction of methyl and methoxy substituents from **a**, to **b**, and **d** the oxidation potential of TPA shifts cathodically while for the Ru center it remains undisturbed. Introduction of trifluoromethyl/methoxy substituents at the cyclometalating ring shifts anodically/cathodically the $\text{Ru}^{3+/2+}$ oxidation potential while not disturbing TPA oxidation potential as seen comparing values for **c**, **e**, and **f**. Data for **c** and **d** versus **b** reveal that dpb is more electron rich cyclometalating ligand than pbpy. The figure is build based on data provided in literature [107,120].



J_{sc} [mA/cm^2]:	14.95	8.26	13.00	16.74
V_{oc} [mV]:	672	608	653	682
FF [%]:	71	77	75	71
PCE [%]:	7.13	3.90	6.33	8.02

Figure 16. Performance of cyclometalated ruthenium sensitizers with tridentate ligands in solar cells [107]. With N3 sensitizer and electrolyte optimized for presented new sensitizers J_{sc} , V_{oc} , FF, and PCE of 16.48 mA/cm^2 , 713 mV, 74%, and 8.65% respectively were achieved. Reported titled for sensitizers are different than in original work.

4. Solar Cells with Co and Cu Electrolytes

Later, new electrolytes based on a single-electron outer-sphere $\text{Co}^{3+}/^{2+}$ redox shuttle were developed for DSC application [121–123]. Organic sensitizers designed to perform with cobalt-based electrolyte soon overrode Ru-complexes providing PCE over 14% as higher V_{OC} in comparison to devices with iodine-based electrolytes were achieved [6,124,125]. In comparison to a solar cell with an iodine-based electrolyte, those with a cobalt-based electrolyte usually suffer from strong charge recombination rates. To reduce the recombination rate, organic sensitizers were suited with long and bulky alkyl chains, which keep the redox shuttle away from the titania surface, while slightly reducing the regeneration yield [126,127]. Ruthenium sensitizers, generally those with isothiocyanate ligands perform poorly with cobalt-based electrolyte. By the means of quantum-mechanical calculations, Mosconi et al. showed that there is a columbic attraction between the N3 sensitizer on the titania surface and a cobalt complex in the electrolyte [128]. This interaction could be responsible for high concentration of redox species near the surface and could hasten recombination rates. Thus, the general thought of community was that ruthenium sensitizers are incompatible with cobalt-based electrolytes. However, Polander et al. introduced a new *tris*-heteroleptic cyclometalated Ru-complex which provided a PCE over 8% with cobalt-based electrolyte. In this work, our group used approach developed for organic sensitizers. In the new *tris*-heteroleptic cyclometalated ruthenium complex, to the ancillary and donating ligands the bulky alkyl chains were attached. Design of a proper ancillary ligand with alkyl chains was fairly simple, in fact the one in C101 sensitizer was selected. However, design of cyclometalating ligands with alkyl chains and with electron-donating power equivalent to that of 2-(2,4-difluorophenyl)-pyridine, to ensure suitable oxidation potential, was effortful. Authors circumvented this problem by derivatizing 2,3'-bipyridine with two dodecyloxy-chains on the 2' and 6' positions (Figure 17). Thus, a strong electron withdrawing character of 2,3'-bipyridine ligand is canceled off by π -electron donating nature of alkoxy chains resulting in a bidentate ligand of suitable electronic properties.

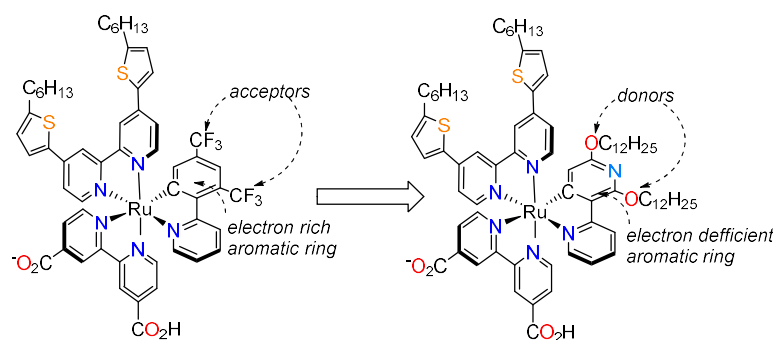


Figure 17. Substitution of 2-(2,6-bis(trifluoromethyl)phenyl)pyridine cyclometalating ligand with 2',6'-bis(dodecyloxy)-2,3'-bipyridine cyclometalating ligand results in a new complex with two additional long alkyl chains and with suitable oxidation potential.

Synthesized *tris*-heteroleptic complex LP1 was compared with its analogue LP0, whereby instead of dodecyloxy, short methoxy substituents were introduced. In a solar cell with LP1, the J_{SC} , V_{OC} , and PCE of 13.2 mA/cm^2 , 837 mV, and 8.6% were obtained. In comparison, with LP0 lower results of 8.3 mA/cm^2 , 714 mV, and 4.7% were obtained (Figure 18) [113]. The higher voltage obtained with LP1 in comparison to LP0 was related to 1.5-fold increased electron recombination lifetime. However, 60% higher J_{SC} obtained with LP1 in comparison to LP0 is surprising. Throughout the whole spectrum, the IPCE obtained for LP0 is ca. 15% lower than that with LP1. Most probably, apart the high electron recombination rates, there are additional sources of low photocurrents obtained with LP0, dye-aggregation and dye-loading just to mention.

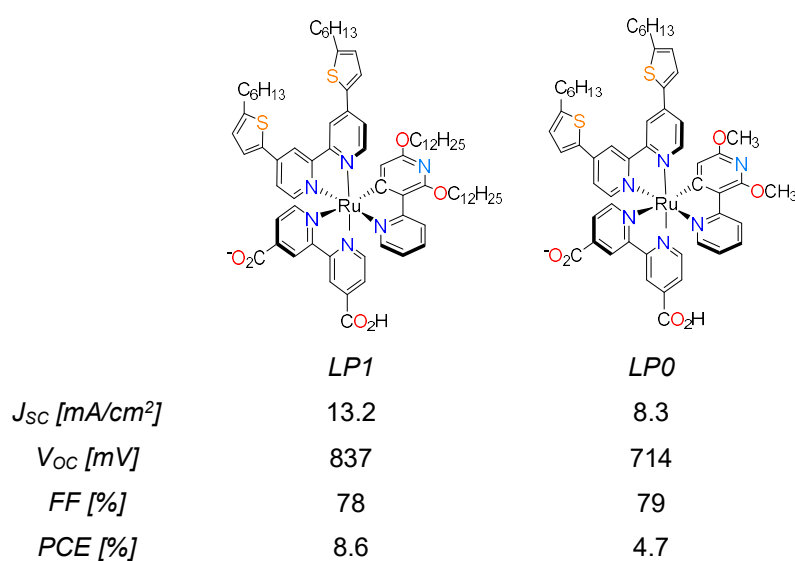


Figure 18. Improved performance of LP1 in comparison to LP0. An electrolyte based on $[Co(phen)_3]^{2+/3+}$ redox was used [113].

Satisfied with these results, we have decided to further investigate the compatibility of ruthenium sensitizers with cobalt-based electrolytes in solar cells. In this course, we have designed six new sensitizers, namely SA22, SA25, SA246, SA282, SA284, and SA285, with various aromatic substituents on the ancillary ligand, and with the same cyclometalating and anchoring ligands as in LP1 (Figure 19) [114]. In solar cells with Co-based electrolyte, SA246 provided the highest PCE of 9.4% as the result of 14.55 mA/cm^2 and 845 mV of photocurrent density and voltage. By the means of electrochemical impedance spectroscopy and transient absorption spectroscopy, we analyzed the timing of different processes taking place. However, obtained results could not explain exceptionally good performance of SA246 with substituents on the ancillary ligand based on thieno-thiophene. Additionally, in this series, SA25 showed the most redshifted absorption spectrum. However, in the end, the dye-loading analysis revealed that SA246 loads onto the titania in much higher amount than other sensitizers in this series (Figure 20). We did not observe any trend between the molecular volume of sensitizer and their loading onto titania. The differences in the nature of aromatic substituents at the ancillary ligands prevented us from making solid conclusions on parameters influencing dye-loading.

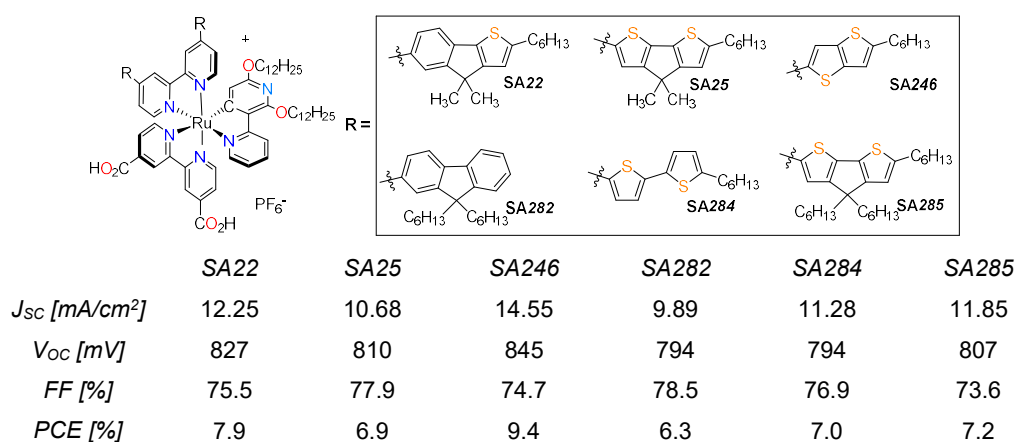


Figure 19. Photovoltaic performance of a series of cyclometalated ruthenium complexes with Co-based electrolyte in DSCs [114].

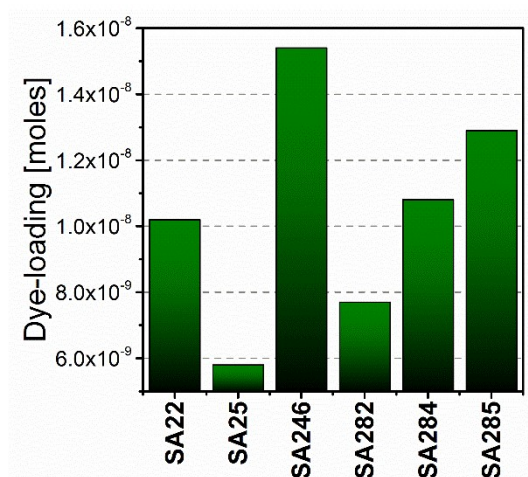


Figure 20. Dye-loading values obtained from the desorption of dyes from sensitized titania films [114].

In the next study, we have further developed three new sensitizers SA633, SA634, and SA635, which have very similar substituents on the ancillary ligand based on diphenyl amine (Figure 21) [115]. In this work, we obtained PCEs in the range of 7.6–8.2%, with the best efficiency achieved with SA634 having phenothiazine substituents. The difference in dye-loading was negligible and the J_{SC} matched well with the current density derived from the IPCE measurements. We related the differences in performances to the obtained V_{OC} which we based purely on electron lifetimes obtained from charge extraction and transient photovoltage decay measurements. Additionally, in both works we have shown that although the organic substituents on the ancillary ligand improve photophysical characteristics of sensitizer, they also impart redox irreversibility. For SA633, SA634, and SA635 with clear two oxidation potentials, with Randles-Sevcik analysis and spectroelectrochemical measurements, we showed that the first oxidation related to the $Ru^{2+/3+}$ is reversible, while the second oxidation related to the organic donor oxidation is irreversible. This observation undermines the well-established tendency in Ru-sensitizer design comprised in attaching various organic moieties to the complex.

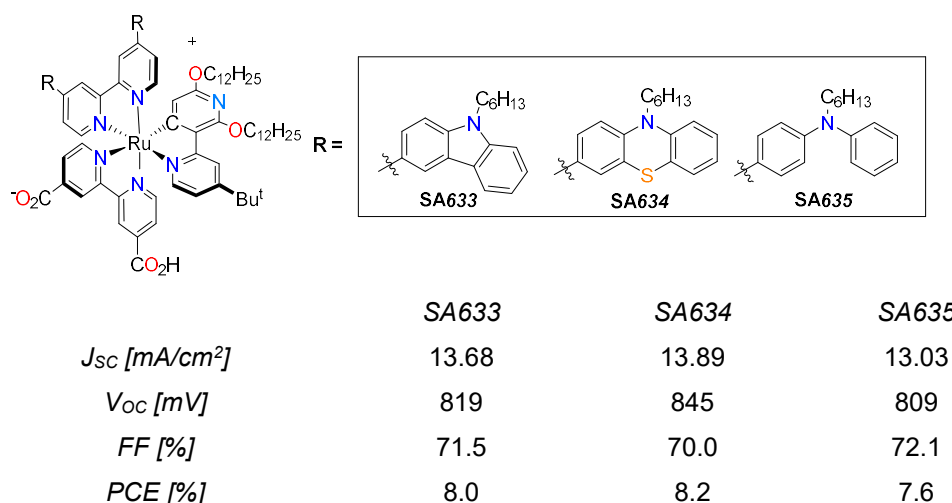


Figure 21. Cyclometalated ruthenium complexes with arylamine electron donating groups and their performance in DSCs with Co-based electrolyte [115].

5. Future Perspectives

Above, we have briefly described the main directions that chemists follow to develop ruthenium sensitizers. In a more general observation, it seems that various groups of complexes where ruthenium is coordinated with different ligands, be it complexes with isothiocyanate, pyridine-pyrazole, or cyclometalating ligands, were actually developed in the same direction and attached organic substituents to the original metal complex. If compared to initial N3 or N719 sensitizer, improvements in PCEs with newer sensitizers were incremental. The positive effect of organic substituents in improving photophysical characteristics of complex is often canceled due to increased molecular volume, resulting in low dye-loadings. Moreover, these organic substituents usually impart instability. Finally, the introduction of organic substituents infers additional synthetic steps, resulting in expensive final products. In this regard, we are advocating for the development of new simple coordination environments to obtain complexes that are suitable for DSC's characteristics. As such, we have obtained preliminary results with new type of *bis*-heteroleptic ruthenium complexes, derivatives of $[\text{Ru}(\text{ppy})(\text{bpy})_2]^+$ in which the pyridine ring of ppy ligand is changed to *N*-heteroleptic carbene (NHC) [129]. This modification let us to control photophysical properties of complex by modifying both cyclometalating and NHC rings. For example, complex SA-x (Figure 22), which we synthesized in a two-step procedure with high yields (Scheme 5), possesses broad absorption spectrum with the onset at 800 nm and extinction coefficients reaching values over $15 \times 10^3 \text{ M}^{-1} \cdot \text{cm}^{-1}$. Moreover, this complex presented absolutely reversible oxidation and reduction potentials with values suitable for standard DSCs. However, hydrolysis of ester groups to yield the final sensitizer resulted in the complex of very low solubility in many standard solvents used for device fabrication. Changing one of the anchoring ligands with simple 2,2'-bipyridine may increase the solubility, and an alternative synthetic procedure should be developed in this regard.

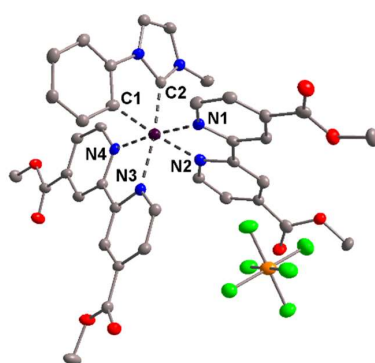
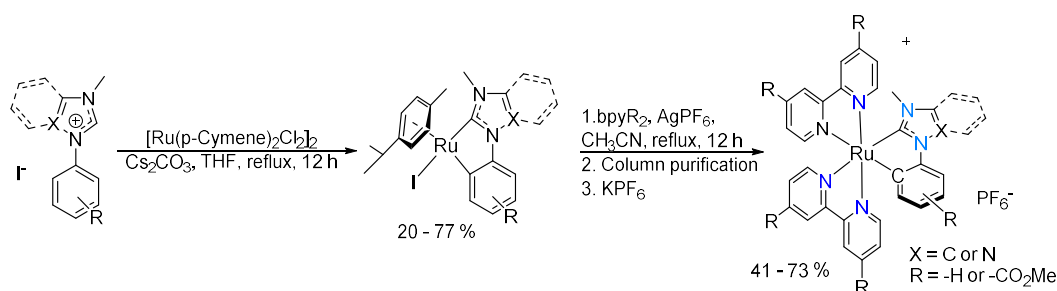


Figure 22. Structural representation of asymmetrical unit of SA-x (hydrogen atoms are omitted for clarity). Color code: Ru—violet; N—blue; C—gray; O—red; P—orange; F—green. Bond distances: Ru-C2 = 2.030(7) Å; Ru-C1 = 2.002(7) Å.



Scheme 5. Synthesis of new cyclometalated ruthenium complexes with *N*-heteroleptic carbene ligands.

Due to the successful performance of ruthenium polypyridine complexes with their MLCT transition and later of D- π -A organic and porphyrin sensitizers with their D-A and π - π^* transitions, other possible alternatives earned less attention. Recently, promising results were obtained with heteroleptic ruthenium diacetylid complexes [130,131]. Regarding the first row transition metals, only copper [132–134] and iron complexes [135,136] have gained a significant attention in the context of sensitization. However, other first row transition metal complexes were missed in the DSC community. Possibilities with first-row transition metals were underlined with examples presented by the group of Heyduk, which reported a series of nickel complexes with redox active ligands and with a very intense interligand D-A charge transfer [137,138].

6. Conclusions

In this short review, we have presented the main classes of ruthenium complexes developed for DSC application. Through the discussion, we have underlined design principles and were critical toward them whenever possible. In general, very high performances were obtained with DSCs using ruthenium complexes. However, already in 1993 a PCE over 10% was achieved with N3 sensitizer, and all improvements later in history were incremental. We and others have developed new sensitizers ignoring the approach from the first principles. Shortly, we need sensitizers with high extinction coefficients, which will homogeneously cover the mesoporous oxide in high dye-loadings. Moreover, we should not sacrifice one of these principles to gain in another, as it was in the last two decades with new sensitizers of high molar absorptivity and high molecular volumes. In general, simple ruthenium complexes possess very broad but not intense enough absorption spectra. To progress the field, we need to look into alternative coordination environments for the ruthenium complexes, or even start intensively looking for metal complexes of first row transition elements.

Funding: The authors acknowledge European Commission H2020-ICT-2014-1, SOLEDLIGHT project, grant number 643791.

Conflicts of Interest: The authors declare no conflicts of interest.

References

1. Gray, H.B. Powering the planet with solar fuel. *Nat. Chem.* **2009**, *1*, 7. [[CrossRef](#)] [[PubMed](#)]
2. Lewis, N.S.; Nocera, D.G. Powering the planet: Chemical challenges in solar energy utilization. *Proc. Natl. Acad. Sci. USA* **2006**, *103*, 15729–15735. [[CrossRef](#)] [[PubMed](#)]
3. O'Regan, B.; Grätzel, M. A low-cost, high-efficiency solar cell based on dye-sensitized colloidal TiO₂ films. *Nature* **1991**, *353*, 737–740. [[CrossRef](#)]
4. Grätzel, M. Solar Energy Conversion by Dye-Sensitized Photovoltaic Cells. *Inorg. Chem.* **2005**, *44*, 6841–6851. [[CrossRef](#)] [[PubMed](#)]
5. Ito, S.; Murakami, T.N.; Comte, P.; Liska, P.; Grätzel, C.; Nazeeruddin, M.K.; Grätzel, M. Fabrication of thin film dye sensitized solar cells with solar to electric power conversion efficiency over 10%. *Thin Solid Films* **2008**, *516*, 4613–4619. [[CrossRef](#)]
6. Kakiage, K.; Aoyama, Y.; Yano, T.; Oya, K.; Fujisawa, J.; Hanaya, M. Highly-efficient dye-sensitized solar cells with collaborative sensitization by silyl-anchor and carboxy-anchor dyes. *Chem. Commun.* **2015**, *51*, 15894–15897. [[CrossRef](#)] [[PubMed](#)]
7. Marcus, R.A. On the Theory of Oxidation-Reduction Reactions Involving Electron Transfer. I. *J. Chem. Phys.* **1956**, *24*, 966–978. [[CrossRef](#)]
8. Marcus, R.A. Electrostatic Free Energy and Other Properties of States Having Nonequilibrium Polarization. I. *J. Chem. Phys.* **1956**, *24*, 979–989. [[CrossRef](#)]
9. Marcus, R.A.; Sutin, N. Electron transfers in chemistry and biology. *Biochim. Biophys. Acta Rev. Bioenergy* **1985**, *811*, 265–322. [[CrossRef](#)]
10. Gerischer, H. Electrochemical Techniques for the Study of Photosensitization. *Photochem. Photobiol.* **1972**, *16*, 243–260. [[CrossRef](#)]

11. Gerischer, H.; Willig, F. Reaction of excited dye molecules at electrodes. In *Physical and Chemical Applications of Dyestuffs*; Springer: Berlin/Heidelberg, Germany, 1976; pp. 31–84. ISBN 978-3-540-38098-6.
12. Ardo, S.; Meyer, G.J. Photodriven heterogeneous charge transfer with transition-metal compounds anchored to TiO₂ semiconductor surfaces. *Chem. Soc. Rev.* **2009**, *38*, 115–164. [[CrossRef](#)] [[PubMed](#)]
13. Shockley, W.; Queisser, H.J. Detailed balance limit of efficiency of p-n junction solar cells. *J. Appl. Phys.* **1961**, *32*, 510–519. [[CrossRef](#)]
14. Hagfeldt, A.; Boschloo, G.; Sun, L.; Kloo, L.; Pettersson, H. Dye-Sensitized Solar Cells. *Chem. Rev.* **2010**, *110*, 6595–6663. [[CrossRef](#)] [[PubMed](#)]
15. Pashaei, B.; Shahroosvand, H.; Grätzel, M.; Nazeeruddin, M.K. Influence of Ancillary Ligands in Dye-Sensitized Solar Cells. *Chem. Rev.* **2016**, *116*, 9485–9564. [[CrossRef](#)] [[PubMed](#)]
16. Orgel, L.E. Double bonding in chelated metal complexes. *J. Chem. Soc.* **1961**, 3683–3686. [[CrossRef](#)]
17. Desilvestro, J.; Grätzel, M.; Kavan, L.; Moser, J.; Augustynski, J. Highly Efficient Sensitization of Titanium Dioxide. *J. Am. Chem. Soc.* **1985**, *107*, 2988–2990. [[CrossRef](#)]
18. Vlachopoulos, N.; Liska, P.; Augustynski, J.; Graetzel, M. Very efficient visible light energy harvesting and conversion by spectral sensitization of high surface area polycrystalline titanium dioxide films. *J. Am. Chem. Soc.* **1988**, *110*, 1216–1220. [[CrossRef](#)]
19. Liska, P.; Vlachopoulos, N.; Nazeeruddin, M.K.; Comte, P.; Gratzel, M. *cis*-Diaquabis(2,2′-bipyridyl-4,4′-dicarboxylate)-ruthenium(II) Sensitizes Wide Band Gap Oxide Semiconductors Very Efficiently over a Broad Spectral Range in the Visible. *J. Am. Chem. Soc.* **1988**, *110*, 3686–3687. [[CrossRef](#)]
20. Amadelli, R.; Argazzi, R.; Bignozzi, C.A.; Scandola, F. Design of Antenna–Sensitizer Polynuclear Complexes. Sensitization of Titanium Dioxide with [Ru(bpy)₂(CN)₂]₂Ru(bpy(COO)₂)₂²⁻. *J. Am. Chem. Soc.* **1990**, *112*, 7099–7103. [[CrossRef](#)]
21. Nazeeruddin, M.K.; Kay, A.; Rodicio, I.; Humphry-Baker, R.; Mueller, E.; Liska, P.; Vlachopoulos, N.; Grätzel, M. Conversion of light to electricity by *cis*-X₂bis(2,2′-bipyridyl-4,4′-dicarboxylate)ruthenium(II) charge-transfer sensitizers (X = Cl⁻, Br⁻, I⁻, CN⁻, and SCN⁻) on nanocrystalline titanium dioxide electrodes. *J. Am. Chem. Soc.* **1993**, *115*, 6382–6390. [[CrossRef](#)]
22. Nazeeruddin, M.K.; Zakeeruddin, S.M.; Humphry-Baker, R.; Jirousek, M.; Liska, P.; Vlachopoulos, N.; Shklover, V.; Fischer, C.-H.; Grätzel, M. Acid–Base Equilibria of (2,2′-Bipyridyl-4,4′-dicarboxylic acid)ruthenium(II) Complexes and the Effect of Protonation on Charge-Transfer Sensitization of Nanocrystalline Titania. *Inorg. Chem.* **1999**, *38*, 6298–6305. [[CrossRef](#)] [[PubMed](#)]
23. Gerischer, H. Neglected problems in the pH dependence of the flatband potential of semiconducting oxides and semiconductors covered with oxide layers. *Electrochim. Acta* **1989**, *34*, 1005–1009. [[CrossRef](#)]
24. Yan, S.G.; Hupp, J.T. Semiconductor-Based Interfacial Electron-Transfer Reactivity: Decoupling Kinetics from pH-Dependent Band Energetics in a Dye-Sensitized Titanium Dioxide/Aqueous Solution System. *J. Phys. Chem.* **1996**, *100*, 6867–6870. [[CrossRef](#)]
25. Nozik, A.J. Photoelectrochemistry: Applications to Solar Energy Conversion. *Annu. Rev. Phys. Chem.* **1978**, *29*, 189–222. [[CrossRef](#)]
26. Huang, S.Y.; Schlichthörl, G.; Nozik, A.J.; Grätzel, M.; Frank, A.J. Charge Recombination in Dye-Sensitized Nanocrystalline TiO₂ Solar Cells. *J. Phys. Chem. B* **1997**, *101*, 2576–2582. [[CrossRef](#)]
27. Nazeeruddin, M.K.; De Angelis, F.; Fantacci, S.; Selloni, A.; Viscardi, G.; Liska, P.; Ito, S.; Takeru, B.; Grätzel, M. Combined experimental and DFT-TDDFT computational study of photoelectrochemical cell ruthenium sensitizers. *J. Am. Chem. Soc.* **2005**, *127*, 16835–16847. [[CrossRef](#)] [[PubMed](#)]
28. Snaith, H.J. Estimating the Maximum Attainable Efficiency in Dye-Sensitized Solar Cells. *Adv. Funct. Mater.* **2010**, *20*, 13–19. [[CrossRef](#)]
29. Koops, S.E.; O’Regan, B.C.; Barnes, P.R.F.; Durrant, J.R. Parameters Influencing the Efficiency of Electron Injection in Dye-Sensitized Solar Cells. *J. Am. Chem. Soc.* **2009**, *131*, 4808–4818. [[CrossRef](#)] [[PubMed](#)]
30. O’Regan, B.C.; Durrant, J.R. Kinetic and Energetic Paradigms for Dye-Sensitized Solar Cells: Moving from the Ideal to the Real. *Acc. Chem. Res.* **2009**, *42*, 1799–1808. [[CrossRef](#)] [[PubMed](#)]
31. Watson, D.F.; Meyer, G.J. Electron Injection at Dye-Sensitized Semiconductor Electrodes. *Annu. Rev. Phys. Chem.* **2005**, *56*, 119–156. [[CrossRef](#)] [[PubMed](#)]
32. Nazeeruddin, M.K.; Péchy, P.; Renouard, T.; Zakeeruddin, S.M.; Humphry-Baker, R.; Comte, P.; Liska, P.; Cevey, L.; Costa, E.; Shklover, V.; et al. Engineering of Efficient Panchromatic Sensitizers for Nanocrystalline TiO₂-Based Solar Cells. *J. Am. Chem. Soc.* **2001**, *123*, 1613–1624. [[CrossRef](#)] [[PubMed](#)]

33. Black, D.S.C.; Deacon, G.B.; Thomas, N.C. New decarbonylation reactions of carbonylruthenium(II) complexes. *Inorg. Chim. Acta* **1982**, *65*, L75–L76. [[CrossRef](#)]
34. St. Black, D.C.; Deacon, G.B.; Thomas, N.C. Ruthenium Carbonyl Complexes. I* Synthesis of $[\text{Ru}(\text{CO})_2(\text{bidentate})_2]^{2+}$ Complexes. *Aust. J. Chem.* **1982**, *35*, 2445–2453. [[CrossRef](#)]
35. Strouse, G.F.; Anderson, P.A.; Schoonover, J.R.; Meyer, T.J.; Keene, F.R. Synthesis of polypyridyl complexes of ruthenium(II) containing three different bidentate ligands. *Inorg. Chem.* **1992**, *31*, 3004–3006. [[CrossRef](#)]
36. Anderson, P.A.; Strouse, G.F.; Treadway, J.A.; Keene, F.R.; Meyer, T.J. Black MLCT Absorbers. *Inorg. Chem.* **1994**, *33*, 3863–3864. [[CrossRef](#)]
37. Anderson, P.A.; Deacon, G.B.; Haarmann, K.H.; Richard Keene, F.; Meyer, T.J.; Reitsma, D.A.; Skelton, B.W.; Strouse, G.F.; Thomas, N.C.; Treadway, J.A.; et al. Designed Synthesis of Mononuclear *Tris*(heteroleptic) Ruthenium Complexes Containing Bidentate Polypyridyl Ligands. *Inorg. Chem.* **1995**, *34*, 6145–6157. [[CrossRef](#)]
38. Zakeeruddin, S.M.; Nazeeruddin, M.K.; Humphry-Baker, R.; Péchy, P.; Quagliotto, P.; Barolo, C.; Viscardi, G.; Grätzel, M. Design, synthesis, and application of amphiphilic ruthenium polypyridyl photosensitizers in solar cells based on nanocrystalline TiO_2 films. *Langmuir* **2002**, *18*, 952–954. [[CrossRef](#)]
39. Freedman, D.A.; Evju, J.K.; Pomije, M.K.; Mann, K.R. Convenient synthesis of *tris*-heteroleptic ruthenium(II) polypyridyl complexes. *Inorg. Chem.* **2001**, *40*, 5711–5715. [[CrossRef](#)] [[PubMed](#)]
40. Zakeeruddin, S.M.; Nazeeruddin, M.K.; Humphry-Baker, R.; Grätzel, M.; Shklover, V. Stepwise Assembly of *Tris*-Heteroleptic Polypyridyl Complexes of Ruthenium(II). *Inorg. Chem.* **1998**, *37*, 5251–5259. [[CrossRef](#)]
41. Wang, P.; Zakeeruddin, S.M.; Moser, J.E.; Nazeeruddin, M.K.; Sekiguchi, T.; Grätzel, M. A stable quasi-solid-state dye-sensitized solar cell with an amphiphilic ruthenium sensitizer and polymer gel electrolyte. *Nat. Mater.* **2003**, *2*, 402–407. [[CrossRef](#)] [[PubMed](#)]
42. Wang, P.; Zakeeruddin, S.M.; Moser, J.E.; Humphry-Baker, R.; Comte, P.; Aranyos, V.; Hagfeldt, A.; Nazeeruddin, M.K.; Grätzel, M. Stable new sensitizer with improved light harvesting for nanocrystalline dye-sensitized solar cells. *Adv. Mater.* **2004**, *16*, 1806–1811. [[CrossRef](#)]
43. Wang, P.; Klein, C.; Humphry-Baker, R.; Zakeeruddin, S.M.; Grätzel, M. A high molar extinction coefficient sensitizer for stable dye-sensitized solar cells. *J. Am. Chem. Soc.* **2005**, *127*, 808–809. [[CrossRef](#)] [[PubMed](#)]
44. Kuang, D.; Ito, S.; Wenger, B.; Klein, C.; Moser, J.E.; Humphry-Baker, R.; Zakeeruddin, S.M.; Grätzel, M. High molar extinction coefficient heteroleptic ruthenium complexes for thin film dye-sensitized solar cells. *J. Am. Chem. Soc.* **2006**, *128*, 4146–4154. [[CrossRef](#)] [[PubMed](#)]
45. Kuang, D.; Klein, C.; Ito, S.; Moser, J.E.; Humphry-Baker, R.; Evans, N.; Duriaux, F.; Grätzel, C.; Zakeeruddin, S.M.; Grätzel, M. High-Efficiency and stable mesoscopic dye-sensitized solar cells based on a high molar extinction coefficient ruthenium sensitizer and nonvolatile electrolyte. *Adv. Mater.* **2007**, *19*, 1133–1137. [[CrossRef](#)]
46. Chen, C.-Y.; Wu, S.-J.; Wu, C.-G.; Chen, J.-G.; Ho, K.-C. A Ruthenium Complex with Superhigh Light-Harvesting Capacity for Dye-Sensitized Solar Cells. *Angew. Chem. Int. Ed.* **2006**, *45*, 5822–5825. [[CrossRef](#)] [[PubMed](#)]
47. Chen, C.-Y.; Wu, S.-J.; Li, J.-Y.; Wu, C.-G.; Chen, J.-G.; Ho, K.-C. A New Route to Enhance the Light-Harvesting Capability of Ruthenium Complexes for Dye-Sensitized Solar Cells. *Adv. Mater.* **2007**, *19*, 3888–3891. [[CrossRef](#)]
48. Gao, F.; Wang, Y.; Shi, D.; Zhang, J.; Wang, M.; Jing, X.; Humphry-Baker, R.; Wang, P.; Zakeeruddin, S.M.; Grätzel, M. Enhance the optical absorptivity of nanocrystalline TiO_2 film with high molar extinction coefficient ruthenium sensitizers for high performance dye-sensitized solar cells. *J. Am. Chem. Soc.* **2008**, *130*, 10720–10728. [[CrossRef](#)] [[PubMed](#)]
49. Yu, Q.; Liu, S.; Zhang, M.; Cai, N.; Wang, Y.; Wang, P. An extremely high molar extinction coefficient ruthenium sensitizer in dye-sensitized solar cells: The effects of π -conjugation extension. *J. Phys. Chem. C* **2009**, *113*, 14559–14566. [[CrossRef](#)]
50. Cao, Y.; Bai, Y.; Yu, Q.; Cheng, Y.; Liu, S.; Shi, D.; Gao, F.; Wang, P. Dye-sensitized solar cells with a high absorptivity ruthenium sensitizer featuring a 2-(hexylthio)thiophene conjugated bipyridine. *J. Phys. Chem. C* **2009**, *113*, 6290–6297. [[CrossRef](#)]
51. Chen, C.Y.; Wang, M.; Li, J.Y.; Pootrakulchote, N.; Alibabaei, L.; Ngoc-Le, C.H.; Decoppet, J.D.; Tsai, J.H.; Grätzel, C.; Wu, C.G.; et al. Highly efficient light-harvesting ruthenium sensitizer for thin-film dye-sensitized solar cells. *ACS Nano* **2009**, *3*, 3103–3109. [[CrossRef](#)] [[PubMed](#)]

52. Karthikeyan, C.S.; Wietasch, H.; Thelakkat, M. Highly efficient solid-state dye-sensitized TiO₂ solar cells using donor-antenna dyes capable of multistep charge-transfer cascades. *Adv. Mater.* **2007**, *19*, 1091–1095. [[CrossRef](#)]
53. Gao, F.; Wang, Y.; Zhang, J.; Shi, D.; Wang, M.; Humphry-Baker, R.; Wang, P.; Zakeeruddin, S.M.; Grätzel, M. A new heteroleptic ruthenium sensitizer enhances the absorptivity of mesoporous titania film for a high efficiency dye-sensitized solar cell. *Chem. Commun.* **2008**, *107*, 2635–2637. [[CrossRef](#)] [[PubMed](#)]
54. Kim, J.J.; Lim, K.; Choi, H.; Fan, S.; Kang, M.S.; Gao, G.; Kang, H.S.; Ko, J. New efficient ruthenium sensitizers with unsymmetrical indeno[1,2-*b*]thiophene or a fused dithiophene ligand for dye-sensitized solar cells. *Inorg. Chem.* **2010**, *49*, 8351–8357. [[CrossRef](#)] [[PubMed](#)]
55. Chen, C.-Y.; Chen, J.-G.; Wu, S.-J.; Li, J.-Y.; Wu, C.-G.; Ho, K.-C. Multifunctionalized ruthenium-based supersensitizers for highly efficient dye-sensitized solar cells. *Angew. Chem. Int. Ed.* **2008**, *47*, 7342–7345. [[CrossRef](#)] [[PubMed](#)]
56. Li, J.-Y.; Chen, C.-Y.; Chen, J.-G.; Tan, C.-J.; Lee, K.-M.; Wu, S.-J.; Tung, Y.-L.; Tsai, H.-H.; Ho, K.-C.; Wu, C.-G. Heteroleptic ruthenium antenna-dye for high-voltage dye-sensitized solar cells. *J. Mater. Chem.* **2010**, *20*, 7158–7164. [[CrossRef](#)]
57. Chen, C.Y.; Pootrakulchote, N.; Wu, S.J.; Wang, M.; Li, J.Y.; Tsai, J.H.; Wu, C.G.; Zakeeruddin, S.M.; Grätzel, M. New ruthenium sensitizer with carbazole antennas for efficient and stable Thin-film Dye-sensitized solar cells. *J. Phys. Chem. C* **2009**, *113*, 20752–20757. [[CrossRef](#)]
58. Choi, H.; Baik, C.; Kim, S.; Kang, M.-S.; Xu, X.; Kang, H.S.; Kang, S.O.; Ko, J.; Nazeeruddin, M.K.; Grätzel, M. Molecular engineering of hybrid sensitizers incorporating an organic antenna into ruthenium complex and their application in solar cells. *New J. Chem.* **2008**, *32*, 2233–2237. [[CrossRef](#)]
59. Mueller, A.V.; Ramos, L.D.; Frin, K.P.M.; de Oliveira, K.T.; Polo, A.S. A high efficiency ruthenium(II) tris-heteroleptic dye containing 4,7-dicarbazole-1,10-phenanthroline for nanocrystalline solar cells. *RSC Adv.* **2016**, *6*, 46487–46494. [[CrossRef](#)]
60. Chen, W.C.; Kong, F.T.; Ghadari, R.; Li, Z.Q.; Guo, F.L.; Liu, X.P.; Huang, Y.; Yu, T.; Hayat, T.; Dai, S.Y. Unravelling the structural-electronic impact of arylamine electron-donating antennas on the performances of efficient ruthenium sensitizers for dye-sensitized solar cells. *J. Power Sources* **2017**, *346*, 71–79. [[CrossRef](#)]
61. Wang, Z.-S.; Huang, C.-H.; Huang, Y.-Y.; Zhang, B.-W.; Xie, P.-H.; Hou, Y.-J.; Ibrahim, K.; Qian, H.-J.; Liu, F.-Q. Photoelectric behavior of nanocrystalline TiO₂ electrode with a novel terpyridyl ruthenium complex. *Sol. Energy Mater. Sol. Cells* **2002**, *71*, 261–271. [[CrossRef](#)]
62. Funaki, T.; Yanagida, M.; Onozawa-Komatsuzaki, N.; Kawanishi, Y.; Kasuga, K.; Sugihara, H. Ruthenium (II) complexes with π expanded ligand having phenylene-ethynylene moiety as sensitizers for dye-sensitized solar cells. *Sol. Energy Mater. Sol. Cells* **2009**, *93*, 729–732. [[CrossRef](#)]
63. Vougioukalakis, G.C.; Stergiopoulos, T.; Kantonis, G.; Kontos, A.G.; Papadopoulos, K.; Stublla, A.; Potvin, P.G.; Falaras, P. Terpyridine- and 2,6-dipyrazinylpyridine-coordinated ruthenium(II) complexes: Synthesis, characterization and application in TiO₂-based dye-sensitized solar cells. *J. Photochem. Photobiol. A Chem.* **2010**, *214*, 22–32. [[CrossRef](#)]
64. Onozawa-Komatsuzaki, N.; Yanagida, M.; Funaki, T.; Kasuga, K.; Sayama, K.; Sugihara, H. Near-IR sensitization of nanocrystalline TiO₂ with a new ruthenium complex having a 2,6-bis(4-carboxyquinolin-2-yl)pyridine ligand. *Inorg. Chem. Commun.* **2009**, *12*, 1212–1215. [[CrossRef](#)]
65. Onozawa-Komatsuzaki, N.; Yanagida, M.; Funaki, T.; Kasuga, K.; Sayama, K.; Sugihara, H. Near-IR dye-sensitized solar cells using a new type of ruthenium complexes having 2,6-bis(quinolin-2-yl)pyridine derivatives. In *Solar Energy Materials and Solar Cells*; North-Holland: Amsterdam, The Netherlands, 2011; Volume 95, pp. 310–314.
66. Yang, S.H.; Wu, K.L.; Chi, Y.; Cheng, Y.M.; Chou, P.T. Tris(thiocyanate) ruthenium(II) sensitizers with functionalized dicarboxyterpyridine for dye-sensitized solar cells. *Angew. Chem. Int. Ed.* **2011**, *50*, 8270–8274. [[CrossRef](#)] [[PubMed](#)]
67. Kimura, M.; Masuo, J.; Tohata, Y.; Obuchi, K.; Masaki, N.; Murakami, T.N.; Koumura, N.; Hara, K.; Fukui, A.; Yamanaka, R.; et al. Improvement of TiO₂/dye/electrolyte interface conditions by positional change of alkyl chains in modified panchromatic Ru complex dyes. *Chem. Eur. J.* **2013**, *19*, 1028–1034. [[CrossRef](#)] [[PubMed](#)]
68. Numata, Y.; Singh, S.P.; Islam, A.; Iwamura, M.; Imai, A.; Nozaki, K.; Han, L. Enhanced light-harvesting capability of a panchromatic Ru(II) sensitizer based on π -extended terpyridine with a 4-methylstyryl group for dye-sensitized solar cells. *Adv. Funct. Mater.* **2013**, *23*, 1817–1823. [[CrossRef](#)]

69. Nguyen, P.T.; Lam, B.X.T.; Andersen, A.R.; Hansen, P.E.; Lund, T. Photovoltaic performance and characteristics of dye-sensitized solar cells prepared with the n719 thermal degradation products $[\text{Ru}(\text{LH})_2(\text{NCS})(4\text{-tert-butylpyridine})][\text{N}(\text{Bu})_4]$ and $[\text{Ru}(\text{LH})_2(\text{NCS})(1\text{-methylbenzimidazole})][\text{N}(\text{Bu})_4]$. *Eur. J. Inorg. Chem.* **2011**, *2011*, 2533–2539. [[CrossRef](#)]
70. Nguyen, P.T.; Degn, R.; Nguyen, H.T.; Lund, T. Thiocyanate ligand substitution kinetics of the solar cell dye Z-907 by 3-methoxypropionitrile and 4-*tert*-butylpyridine at elevated temperatures. *Sol. Energy Mater. Sol. Cells* **2009**, *93*, 1939–1945. [[CrossRef](#)]
71. Nguyen, H.T.; Ta, H.M.; Lund, T. Thermal thiocyanate ligand substitution kinetics of the solar cell dye N719 by acetonitrile, 3-methoxypropionitrile, and 4-*tert*-butylpyridine. *Sol. Energy Mater. Sol. Cells* **2007**, *91*, 1934–1942. [[CrossRef](#)]
72. Abbotto, A.; Coluccini, C.; Dell’Orto, E.; Manfredi, N.; Trifiletti, V.; Salamone, M.M.; Ruffo, R.; Acciarri, M.; Colombo, A.; Dragonetti, C.; et al. Thiocyanate-free cyclometalated ruthenium sensitizers for solar cells based on heteroaromatic-substituted 2-arylpyridines. *Dalton Trans.* **2012**, *41*, 11731–11738. [[CrossRef](#)] [[PubMed](#)]
73. Dragonetti, C.; Valore, A.; Colombo, A.; Roberto, D.; Trifiletti, V.; Manfredi, N.; Salamone, M.M.; Ruffo, R.; Abbotto, A. A new thiocyanate-free cyclometalated ruthenium complex for dye-sensitized solar cells: Beneficial effects of substitution on the cyclometalated ligand. *J. Organomet. Chem.* **2012**, *714*, 88–93. [[CrossRef](#)]
74. Dragonetti, C.; Colombo, A.; Magni, M.; Mussini, P.; Nisic, F.; Roberto, D.; Ugo, R.; Valore, A.; Valsecchi, A.; Salvatori, P.; et al. Thiocyanate-free ruthenium(II) sensitizer with a pyrid-2-yltetrazolate ligand for dye-sensitized solar cells. *Inorg. Chem.* **2013**, *52*, 10723–10725. [[CrossRef](#)] [[PubMed](#)]
75. Colombo, A.; Dragonetti, C.; Valore, A.; Coluccini, C.; Manfredi, N.; Abbotto, A. Thiocyanate-free ruthenium(II) 2,2'-bipyridyl complexes for dye-sensitized solar cells. *Polyhedron* **2014**, *82*, 50–56. [[CrossRef](#)]
76. Colombo, A.; Dragonetti, C.; Magni, M.; Meroni, D.; Ugo, R.; Marotta, G.; Grazia Lobello, M.; Salvatori, P.; De Angelis, F. New thiocyanate-free ruthenium(II) sensitizers with different pyrid-2-yl tetrazolate ligands for dye-sensitized solar cells. *Dalton Trans.* **2015**, *44*, 11788–11796. [[CrossRef](#)] [[PubMed](#)]
77. Wu, K.-L.; Hsu, H.-C.; Chen, K.; Chi, Y.; Chung, M.-W.; Liu, W.-H.; Chou, P.-T. Development of thiocyanate-free, charge-neutral Ru(II) sensitizers for dye-sensitized solar cells. *Chem. Commun.* **2010**, *46*, 5124–5126. [[CrossRef](#)] [[PubMed](#)]
78. Wang, S.-W.; Wu, K.-L.; Ghadiri, E.; Lobello, M.G.; Ho, S.-T.; Chi, Y.; Moser, J.-E.; De Angelis, F.; Grätzel, M.; Nazeeruddin, M.K. Engineering of thiocyanate-free Ru(II) sensitizers for high efficiency dye-sensitized solar cells. *Chem. Sci.* **2013**, *4*, 2423–2433. [[CrossRef](#)]
79. Wu, K.-L.; Ku, W.-P.; Clifford, J.N.; Palomares, E.; Ho, S.-T.; Chi, Y.; Liu, S.-H.; Chou, P.-T.; Nazeeruddin, M.K.; Grätzel, M. Harnessing the open-circuit voltage via a new series of Ru(II) sensitizers bearing (iso-)quinolinyl pyrazolate ancillaries. *Energy Environ. Sci.* **2013**, *6*, 859–870. [[CrossRef](#)]
80. Moehl, T.; Tsao, H.N.; Wu, K.L.; Hsu, H.C.; Chi, Y.; Ronca, E.; De Angelis, F.; Nazeeruddin, M.K.; Grätzel, M. High open-circuit voltages: Evidence for a sensitizer-induced TiO_2 conduction band shift in Ru(II)-dye sensitized solar cells. *Chem. Mater.* **2013**, *25*, 4497–4502. [[CrossRef](#)]
81. Chen, B.-S.; Chen, K.; Hong, Y.-H.; Liu, W.-H.; Li, T.-H.; Lai, C.-H.; Chou, P.-T.; Chi, Y.; Lee, G.-H. Neutral, panchromatic Ru(II) terpyridine sensitizers bearing pyridine pyrazolate chelates with superior DSSC performance. *Chem. Commun.* **2009**, *0*, 5844–5846. [[CrossRef](#)] [[PubMed](#)]
82. Wang, S.-W.; Chou, C.-C.; Hu, F.-C.; Wu, K.-L.; Chi, Y.; Clifford, J.N.; Palomares, E.; Liu, S.-H.; Chou, P.-T.; Wei, T.-C.; et al. Panchromatic Ru(II) sensitizers bearing single thiocyanate for high efficiency dye sensitized solar cells. *J. Mater. Chem. A* **2014**, *2*, 17618–17627. [[CrossRef](#)]
83. Chou, C.C.; Wu, K.L.; Chi, Y.; Hu, W.P.; Yu, S.J.; Lee, G.H.; Lin, C.L.; Chou, P.T. Ruthenium(II) sensitizers with heteroleptic tridentate chelates for dye-sensitized solar cells. *Angew. Chem. Int. Ed.* **2011**, *50*, 2054–2058. [[CrossRef](#)] [[PubMed](#)]
84. Wu, K.L.; Li, C.H.; Chi, Y.; Clifford, J.N.; Cabau, L.; Palomares, E.; Cheng, Y.M.; Pan, H.A.; Chou, P.T. Dye molecular structure device open-circuit voltage correlation in Ru(II) sensitizers with heteroleptic tridentate chelates for dye-sensitized solar cells. *J. Am. Chem. Soc.* **2012**, *134*, 7488–7496. [[CrossRef](#)] [[PubMed](#)]
85. Chou, C.C.; Hu, F.C.; Yeh, H.H.; Wu, H.P.; Chi, Y.; Clifford, J.N.; Palomares, E.; Liu, S.H.; Chou, P.T.; Lee, G.H. Highly efficient dye-sensitized solar cells based on panchromatic ruthenium sensitizers with quinolinylbipyridine anchors. *Angew. Chem. Int. Ed.* **2014**, *53*, 178–183. [[CrossRef](#)] [[PubMed](#)]

86. Chi, Y.; Wu, K.-L.; Wei, T.-C. Ruthenium and Osmium Complexes That Bear Functional Azolate Chelates for Dye-Sensitized Solar Cells. *Chem. Asian J.* **2015**, *10*, 1098–1115. [[CrossRef](#)] [[PubMed](#)]
87. Reveco, P.; Medley, J.H.; Garber, A.R.; Bhacca, N.S.; Selbin, J. Study of a Cyclometalated Complex of Ruthenium by 400-MHz Two-Dimensional Proton NMR. *Inorg. Chem.* **1985**, *24*, 1096–1099. [[CrossRef](#)]
88. Reveco, P.; Schmehl, R.H.; Cherry, W.R.; Fronczek, F.R.; Selbin, J. Cyclometalated complexes of ruthenium. 2. Spectral and electrochemical properties and X-ray structure of bis(2,2'-bipyridine)(4-nitro-2-(2-pyridyl)phenyl)ruthenium(II). *Inorg. Chem.* **1985**, *24*, 4078–4082. [[CrossRef](#)]
89. Reveco, P.; Cherry, W.R.; Medley, J.; Garber, A.; Gale, R.J.; Selbin, J. Cyclometalated Complexes of Ruthenium. 3. Spectral, Electrochemical, and Two-Dimensional Proton NMR of $[\text{Ru}(\text{bpy})_2(\text{cyclometalating ligand})]^+$. *Inorg. Chem.* **1986**, *25*, 1842–1845. [[CrossRef](#)]
90. Constable, E.C.; Holmes, J.M. A cyclometalated analogue of tris(2,2'-bipyridine)ruthenium(II). *J. Organomet. Chem.* **1986**, *301*, 203–208. [[CrossRef](#)]
91. Collin, J.P.; Beley, M.; Sauvage, J.P.; Barigelletti, F. A room temperature luminescent cyclometalated ruthenium(II) complex of 6-phenyl-2,2'-bipyridine. *Inorg. Chim. Acta* **1991**, *186*, 91–93. [[CrossRef](#)]
92. Barigelletti, F.; Ventura, B.; Collin, J.-P.; Kayhanian, R.; Gavina, P.; Sauvage, J.-P. Electrochemical and spectroscopic properties of cyclometalated and non-cyclometalated ruthenium(II) complexes containing sterically hindering ligands of the phenanthroline and terpyridine families. *Eur. J. Inorg. Chem.* **2000**, *2000*, 113–119. [[CrossRef](#)]
93. Ott, S.; Borgström, M.; Hammarström, L.; Johansson, O. Rapid energy transfer in bichromophoric tris-bipyridyl/cyclometalated ruthenium(II) complexes. *Dalton Trans.* **2006**, 1434–1443. [[CrossRef](#)] [[PubMed](#)]
94. Wadman, S.H.; Lutz, M.; Tooke, D.M.; Spek, A.L.; František Hartl; Havenith, R.W.A.; Van Klink, G.P.M.; Van Koten, G. Consequences of *N,C,N'*- and *C,N,N'*-coordination modes on electronic and photophysical properties of cyclometalated aryl ruthenium(II) complexes. *Inorg. Chem.* **2009**, *48*, 1887–1900. [[CrossRef](#)] [[PubMed](#)]
95. Wadman, S.H.; Van Leeuwen, Y.M.; Havenith, R.W.A.; Van Klink, G.P.M.; Van Koten, G. A redox asymmetric, cyclometalated ruthenium dimer: Toward upconversion dyes in dye-sensitized TiO_2 solar cells. *Organometallics* **2010**, *29*, 5635–5645. [[CrossRef](#)]
96. Borgström, M.; Ott, S.; Lomoth, R.; Bergquist, J.; Hammarström, L.; Johansson, O. Photoinduced energy transfer coupled to charge separation in a Ru(II)-Ru(II)-acceptor triad. *Inorg. Chem.* **2006**, *45*, 4820–4829. [[CrossRef](#)] [[PubMed](#)]
97. Koizumi, T.A.; Tomon, T.; Tanaka, K. Terpyridine-analogous (*N,N,C*)-Tridentate ligands: Synthesis, structures, and electrochemical properties of ruthenium(II) complexes bearing tridentate pyridinium and pyridinylidene ligands. *Organometallics* **2003**, *22*, 970–975. [[CrossRef](#)]
98. Wadman, S.H.; Kroon, J.M.; Bakker, K.; Lutz, M.; Spek, A.L.; van Klink, G.P.M.; van Koten, G. Cyclometalated ruthenium complexes for sensitizing nanocrystalline TiO_2 solar cells. *Chem. Commun.* **2007**, 1907–1909. [[CrossRef](#)]
99. Wadman, S.H.; Kroon, J.M.; Bakker, K.; Havenith, R.W.A.; Van Klink, G.P.M.; Van Koten, G. Cyclometalated organoruthenium complexes for application in dye-sensitized solar cells. *Organometallics* **2010**, *29*, 1569–1579. [[CrossRef](#)]
100. Kreitner, C.; Mengel, A.K.C.; Lee, T.K.; Cho, W.; Char, K.; Kang, Y.S.; Heinze, K. Strongly Coupled Cyclometalated Ruthenium Triarylamine Chromophores as Sensitizers for DSSCs. *Chem. Eur. J.* **2016**, *22*, 8915–8928. [[CrossRef](#)] [[PubMed](#)]
101. Kreitner, C.; Heinze, K. The photochemistry of mono- and dinuclear cyclometalated bis(tridentate)ruthenium(II) complexes: Dual excited state deactivation and dual emission. *Dalton Trans.* **2016**, *45*, 5640–5658. [[CrossRef](#)] [[PubMed](#)]
102. Yao, C.J.; Nie, H.J.; Yang, W.W.; Shao, J.Y.; Yao, J.; Zhong, Y.W. Strongly coupled cyclometalated ruthenium-triarylamine hybrids: Tuning electrochemical properties, intervalence charge transfer, and spin distribution by substituent effects. *Chem. Eur. J.* **2014**, *20*, 17466–17477. [[CrossRef](#)] [[PubMed](#)]
103. Katagiri, S.; Sakamoto, R.; Maeda, H.; Nishimori, Y.; Kurita, T.; Nishihara, H. Terminal redox-site effect on the long-range electron conduction of $\text{Fe}(\text{tpy})_2$ oligomer wires on a gold electrode. *Chem. Eur. J.* **2013**, *19*, 5088–5096. [[CrossRef](#)] [[PubMed](#)]
104. Aghazada, S.; Zimmermann, I.; Ren, Y.; Wang, P.; Nazeeruddin, M.K. Bis-Tridentate-Cyclometalated Ruthenium Complexes with Extended Anchoring Ligand and Their Performance in Dye-Sensitized Solar Cells. *ChemistrySelect* **2018**, *3*, 1585–1592. [[CrossRef](#)]

105. Bomben, P.G.; Robson, K.C.D.; Sedach, P.A.; Berlinguette, C.P. On the viability of cyclometalated Ru(II) complexes for light-harvesting applications. *Inorg. Chem.* **2009**, *48*, 9631–9643. [[CrossRef](#)] [[PubMed](#)]
106. Bonnefous, C.; Chouai, A.; Thummel, R.P. Cyclometalated complexes of Ru(II) with 2-aryl derivatives of quinoline and 1,10-phenanthroline. *Inorg. Chem.* **2001**, *40*, 5851–5859. [[CrossRef](#)] [[PubMed](#)]
107. Robson, K.C.D.; Koivisto, B.D.; Yella, A.; Spornova, B.; Nazeeruddin, M.K.; Baumgartner, T.; Grätzel, M.; Berlinguette, C.P. Design and development of functionalized cyclometalated ruthenium chromophores for light-harvesting applications. *Inorg. Chem.* **2011**, *50*, 5494–5508. [[CrossRef](#)] [[PubMed](#)]
108. Wadman, S.H.; Havenith, R.W.A.; Hartl, F.; Lutz, M.; Spek, A.L.; Van Klink, G.P.M.; Van Koten, G. Redox chemistry and electronic properties of 2,3,5,6-tetrakis(2-pyridyl) pyrazine-bridged diruthenium complexes controlled by *N,C,N'*-biscyclometalated ligands. *Inorg. Chem.* **2009**, *48*, 5685–5696. [[CrossRef](#)] [[PubMed](#)]
109. Fetzer, L.; Boff, B.; Ali, M.; Xiangjun, M.; Collin, J.-P.; Sirlin, C.; Gaiddon, C.; Pfeffer, M. Library of second-generation cycloruthenated compounds and evaluation of their biological properties as potential anticancer drugs: Passing the nanomolar barrier. *Dalton Trans.* **2011**, *40*, 8869–8878. [[CrossRef](#)] [[PubMed](#)]
110. Ji, Z.; Wu, Y. Photoinduced electron transfer dynamics of cyclometalated ruthenium (II)-naphthalenediimide dyad at NiO photocathode. *J. Phys. Chem. C* **2013**, *117*, 18315–18324. [[CrossRef](#)]
111. Bessho, T.; Yoneda, E.; Yum, J.H.; Guglielmi, M.; Tavernelli, L.; Lmai, H.; Rothlisberger, U.; Nazeeruddin, M.K.; Grätzel, M. New paradigm in molecular engineering of sensitizers for solar cell applications. *J. Am. Chem. Soc.* **2009**, *131*, 5930–5934. [[CrossRef](#)] [[PubMed](#)]
112. Bomben, P.G.; Koivisto, B.D.; Berlinguette, C.P. Cyclometalated Ru complexes of type $[Ru^{II}(N^N)_2(C^N)]^z$: Physicochemical response to substituents installed on the anionic ligand. *Inorg. Chem.* **2010**, *49*, 4960–4971. [[CrossRef](#)] [[PubMed](#)]
113. Polander, L.E.; Yella, A.; Curchod, B.F.E.; Ashari Astani, N.; Teuscher, J.; Scopelliti, R.; Gao, P.; Mathew, S.; Moser, J.-E.; Tavernelli, I.; et al. Towards Compatibility between Ruthenium Sensitizers and Cobalt Electrolytes in Dye-Sensitized Solar Cells. *Angew. Chem. Int. Ed.* **2013**, *52*, 8731–8735. [[CrossRef](#)] [[PubMed](#)]
114. Aghazada, S.; Gao, P.; Yella, A.; Marotta, G.; Moehl, T.; Teuscher, J.; Moser, J.-E.; De Angelis, F.; Grätzel, M.; Nazeeruddin, M.K. Ligand Engineering for the Efficient Dye-Sensitized Solar Cells with Ruthenium Sensitizers and Cobalt Electrolytes. *Inorg. Chem.* **2016**, *55*, 6653–6659. [[CrossRef](#)] [[PubMed](#)]
115. Aghazada, S.; Ren, Y.; Wang, P.; Nazeeruddin, M.K. Effect of Donor Groups on the Performance of Cyclometalated Ruthenium Sensitizers in Dye-Sensitized Solar Cells. *Inorg. Chem.* **2017**, *56*, 13437–13445. [[CrossRef](#)] [[PubMed](#)]
116. Bomben, P.G.; Gordon, T.J.; Schott, E.; Berlinguette, C.P. A trisheteroleptic cyclometalated Ru^{II} sensitizer that enables high power output in a dye-sensitized solar cell. *Angew. Chem. Int. Ed.* **2011**, *50*, 10682–10685. [[CrossRef](#)] [[PubMed](#)]
117. Bomben, P.G.; Borau-Garcia, J.; Berlinguette, C.P. Three is not a crowd: Efficient sensitization of TiO₂ by a bulky trichromic trisheteroleptic cycloruthenated dye. *Chem. Commun.* **2012**, *48*, 5599–5601. [[CrossRef](#)] [[PubMed](#)]
118. Motley, T.C.; Troian-Gautier, L.; Brennaman, M.K.; Meyer, G.J. Excited-State Decay Pathways of *Tris*(bidentate) Cyclometalated Ruthenium(II) Compounds. *Inorg. Chem.* **2017**, *56*, 13579–13592. [[CrossRef](#)] [[PubMed](#)]
119. Robson, K.C.D.; Koivisto, B.D.; Berlinguette, C.P. Derivatization of bichromic cyclometalated Ru(II) complexes with hydrophobic substituents. *Inorg. Chem.* **2012**, *51*, 1501–1507. [[CrossRef](#)] [[PubMed](#)]
120. Robson, K.C.D.; Spornova, B.; Koivisto, B.D.; Schott, E.; Brown, D.G.; Berlinguette, C.P. Systematic modulation of a bichromic cyclometalated ruthenium(II) scaffold bearing a redox-active triphenylamine constituent. *Inorg. Chem.* **2011**, *50*, 6019–6028. [[CrossRef](#)] [[PubMed](#)]
121. Nusbaumer, H.; Moser, J.-E.; Shaik, M.Z.; Nazeeruddin, M.K.; Grätzel, M. Co^{II}(dbbip)²⁺ Complex Rivals Tri-iodide/Iodide Redox Mediator in Dye-Sensitized Photovoltaic Cells. *J. Phys. Chem. B* **2001**, *105*, 10461–10464. [[CrossRef](#)]
122. Feldt, S.M.; Wang, G.; Boschloo, G.; Hagfeldt, A. Effects of Driving Forces for Recombination and Regeneration on the Photovoltaic Performance of Dye-Sensitized Solar Cells using Cobalt Polypyridine Redox Couples. *J. Phys. Chem. C* **2011**, *115*, 21500–21507. [[CrossRef](#)]
123. Yum, J.-H.; Baranoff, E.; Kessler, F.; Moehl, T.; Ahmad, S.; Bessho, T.; Marchioro, A.; Ghadiri, E.; Moser, J.-E.; Yi, C.; et al. A cobalt complex redox shuttle for dye-sensitized solar cells with high open-circuit potentials. *Nat. Commun.* **2012**, *3*, 631. [[CrossRef](#)] [[PubMed](#)]

124. Yella, A.; Lee, H.-W.; Tsao, H.N.; Yi, C.; Chandiran, A.K.; Nazeeruddin, M.K.; Diau, E.W.-G.; Yeh, C.-Y.; Zakeeruddin, S.M.; Grätzel, M. Porphyrin-Sensitized Solar Cells with Cobalt (II/III)-Based Redox Electrolyte Exceed 12 Percent Efficiency. *Science* **2011**, *334*, 629–634. [[CrossRef](#)] [[PubMed](#)]
125. Mathew, S.; Yella, A.; Gao, P.; Humphry-Baker, R.; Curchod, B.F.E.; Ashari-Astani, N.; Tavernelli, I.; Rothlisberger, U.; Nazeeruddin, M.K.; Grätzel, M. Dye-sensitized solar cells with 13% efficiency achieved through the molecular engineering of porphyrin sensitizers. *Nat. Chem.* **2014**, *6*, 242–247. [[CrossRef](#)] [[PubMed](#)]
126. Feldt, S.M.; Lohse, P.W.; Kessler, F.; Nazeeruddin, M.K.; Grätzel, M.; Boschloo, G.; Hagfeldt, A. Regeneration and recombination kinetics in cobalt polypyridine based dye-sensitized solar cells, explained using Marcus theory. *Phys. Chem. Chem. Phys.* **2013**, *15*, 7087–7097. [[CrossRef](#)] [[PubMed](#)]
127. Feldt, S.M.; Gibson, E.A.; Gabrielsson, E.; Sun, L.; Boschloo, G.; Hagfeldt, A. Design of organic dyes and cobalt polypyridine redox mediators for high-efficiency dye-sensitized solar cells. *J. Am. Chem. Soc.* **2010**, *132*, 16714–16724. [[CrossRef](#)] [[PubMed](#)]
128. Mosconi, E.; Yum, J.-H.; Kessler, F.; Gómez García, C.J.; Zuccaccia, C.; Cinti, A.; Nazeeruddin, M.K.; Grätzel, M.; De Angelis, F. Cobalt Electrolyte/Dye Interactions in Dye-Sensitized Solar Cells: A Combined Computational and Experimental Study. *J. Am. Chem. Soc.* **2012**, *134*, 19438–19453. [[CrossRef](#)] [[PubMed](#)]
129. Aghazada, S.; Zimmermann, I.; Scutelnic, V.; Nazeeruddin, M.K. Synthesis and Photophysical Characterization of Cyclometalated Ruthenium Complexes with *N*-Heterocyclic Carbene Ligands. *Organometallics* **2017**, *36*, 2397–2403. [[CrossRef](#)]
130. De Sousa, S.; Ducasse, L.; Kauffmann, B.; Toupance, T.; Olivier, C. Functionalization of a ruthenium-diacetylide organometallic complex as a next-generation push-pull chromophore. *Chem. Eur. J.* **2014**, *20*, 7017–7024. [[CrossRef](#)] [[PubMed](#)]
131. De Sousa, S.; Lyu, S.; Ducasse, L.; Toupance, T.; Olivier, C. Tuning visible-light absorption properties of Ru-diacetylide complexes: Simple access to colorful efficient dyes for DSSCs. *J. Mater. Chem. A* **2015**, *3*, 18256–18264. [[CrossRef](#)]
132. Brauchli, S.Y.; Malzner, F.J.; Constable, E.C.; Housecroft, C.E. Copper(I)-based dye-sensitized solar cells with sterically demanding anchoring ligands: Bigger is not always better. *RSC Adv.* **2015**, *5*, 48516–48525. [[CrossRef](#)]
133. Housecroft, C.E.; Constable, E.C. The emergence of copper(I)-based dye sensitized solar cells. *Chem. Soc. Rev.* **2015**, *44*, 8386–8398. [[CrossRef](#)] [[PubMed](#)]
134. Sandroni, M.; Favereau, L.; Planchat, A.; Akdas-Kilig, H.; Szuwarski, N.; Pellegrin, Y.; Blart, E.; Le Bozec, H.; Boujtita, M.; Odobel, F. Heteroleptic copper(I)-polypyridine complexes as efficient sensitizers for dye sensitized solar cells. *J. Mater. Chem. A* **2014**, *2*, 9944–9947. [[CrossRef](#)]
135. Liu, L.; Duchanois, T.; Etienne, T.; Monari, A.; Beley, M.; Assfeld, X.; Haacke, S.; Gros, P.C. A new record excited state 3MLCT lifetime for metalorganic iron(II) complexes. *Phys. Chem. Chem. Phys.* **2016**, *18*, 12550–12556. [[CrossRef](#)] [[PubMed](#)]
136. Monat, J.E.; McCusker, J.K. Femtosecond excited-state dynamics of an iron(II) polypyridyl solar cell sensitizer model. *J. Am. Chem. Soc.* **2000**, *122*, 4092–4097. [[CrossRef](#)]
137. Kramer, W.W.; Cameron, L.A.; Zarkesh, R.A.; Ziller, J.W.; Heyduk, A.F. Donor-acceptor ligand-to-ligand charge-transfer coordination complexes of nickel(II). *Inorg. Chem.* **2014**, *53*, 8825–8837. [[CrossRef](#)] [[PubMed](#)]
138. Cameron, L.A.; Ziller, J.W.; Heyduk, A.F. Near-IR absorbing donor-acceptor ligand-to-ligand charge-transfer complexes of nickel(II). *Chem. Sci.* **2016**, *7*, 1807–1814. [[CrossRef](#)] [[PubMed](#)]

